BIOCHEMISTRY
including biophysical chemistry & molecular biology

Article

pubs.acs.org/biochemistry

Thermodynamics of Nucleic Acid "Shape Readout" by an Aminosugar

Hongjuan Xi, Erik Davis, Nihar Ranjan, Liang Xue,[†] David Hyde-Volpe, and Dev P. Arya*

Laboratory of Medicinal Chemistry, Department of Chemistry, Clemson University, Clemson, South Carolina 29634, United States

Supporting Information

ABSTRACT: Recognition of nucleic acids is important for our understanding of nucleic acid structure as well as for our understanding of nucleic acid–protein interactions. In addition to the direct readout mechanisms of nucleic acids such as H-bonding, shape recognition of nucleic acids is being increasingly recognized as playing an equally important role in DNA recognition. Competition dialysis, UV, flourescent intercalator displacement (FID), computational docking, and calorimetry studies were conducted to study the interaction of neomycin with a variety of nucleic acid conformations (shapes). At pH 5.5, the results suggest the following. (1) Neomycin binds three RNA structures [16S A site rRNA, poly(rA)·poly(rA), and poly(rA)·poly(rU)] with high affinities ($K_a \sim 10^7$ M^{-1}). (2) The binding of neomycin to A-form GC-rich oligomer $d(A_2G_{15}C_{15}T_2)_2$ has an affinity comparable to those of RNA structures. (3) The binding of neomycin to DNA·RNA hybrids shows a 3-fold variance that can be attributed to their structural differences [for poly(dA)·poly(rU), $K_a = 9.4 \times 10^6$ M^{-1}, and for poly(rA)·poly(dT), $K_a = 3.1 \times 10^6$ M^{-1}]. (4) The interaction of neomycin with DNA triplex poly(dA)·2poly(dT) yields a binding affinity (K_a) of 2.4×10^5 M^{-1}. (5) Poly(dA-dT)$_2$ shows the lowest association constant for all nucleic acids studied ($K_a < 10^5$). (6) Neomycin binds to G-quadruplexes with K_a values of $\sim 10^4$–10^5 M^{-1}. (7) Computational studies show that the decrease in major groove width in the B to A transition correlates with increasing neomycin affinity. Neomycin's affinity for various nucleic acid structures can be ranked as follows: RNAs and GC-rich $d(A_2G_{15}C_{15}T_2)_2$ structures > poly(dA)·poly(rU) > poly(rA)·poly(dT) > T·A-T triplex, G-quadruplex, B-form AT-rich, or GC-rich DNA sequences. The results illustrate the first example of a small molecule-based "shape readout" of different nucleic acid conformations.

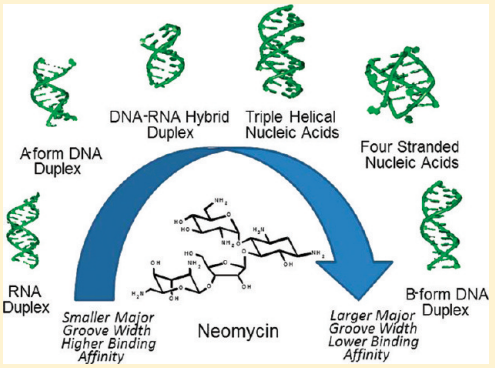

Aminoglycoside antibiotics are well-known chemotherapeutic agents that have been in clinical use for more than six decades.[1] Their activity against *Mycobacterium tuberculosis* and other microorganisms has established them as life-saving drugs and aided significantly in the near eradication of tuberculosis. Aminoglycosides are known to bind to the 16S rRNA subunit of the bacterial ribosome at the A-site and cause erroneous translation leading to disruption of protein synthesis in bacteria. The recent advancements in structural elucidations of aminoglycoside–RNA interactions[2−4] have greatly improved our understanding of their recognition and have revealed that bulged RNA sites serve as the most preferred binding sites for aminoglycosides. Thermodynamics of an aminosugar binding to RNA and DNA sites have been investigated in the past decade.[5−7] Combined with the knowledge obtained from structural studies, ligand–nucleic acid thermodynamics is important for a deeper understanding of small molecule binding, which can be further used for the development of more efficient nucleic acid binding ligands.

Aminoglycoside–nucleic acid recognition studies have primarily centered on binding to ribosomal targets because the ribosome is the site of antibiotic action.[8] There are other nucleic acid structural forms such as triplex, quadruplex, and hybrid structures (Figure 1) that play significant biological roles in a number of cellular processes and have been shown to bind aminoglycosides.[9,10] The binding of small molecules to nucleic acids and subsequent inhibition of their biological functions is a widely accepted strategy for the development of novel therapeutics. For example, targeting duplex DNA can inhibit DNA-protein interactions.[11,12] Binding of aminoglycosides to DNA triplex targets has also been reported.[13] Targeting triplexes has been the focus of antigene strategy for gene regulation,[14−16] while interaction of the ligand with the quadruplex can be utilized to inhibit the function of telomerase and disfavor the interactions of telomere end binding proteins.[16−19] On the other hand, targeting DNA·RNA hybrids such as Okazaki fragments, which are transiently formed during the DNA replication, may also be useful for inhibiting transcription.[20] The studies in our laboratory have shown that binding of aminoglycosides leads to remarkable thermal stabilization of both DNA and RNA triple helices[21] and can induce hybrid triple helix formation.[22] Other examples of DNA·RNA hybrids have been observed in the reverse

Received: July 12, 2011
Revised: August 21, 2011
Published: August 25, 2011

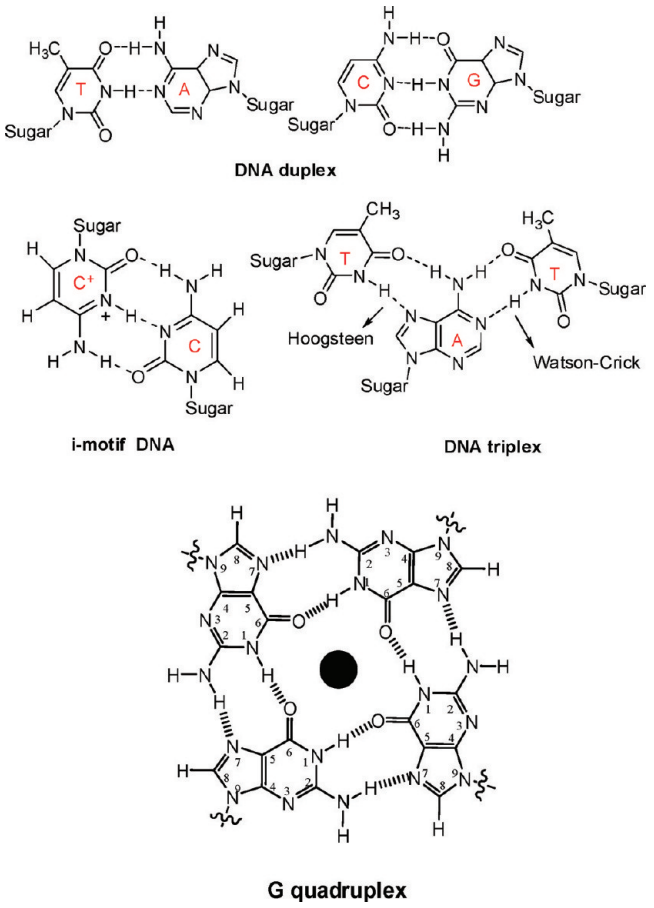

Figure 1. Representative hydrogen bonding patterns formed by the DNA duplex, triplex, and G-quadruplex studied here.

transcription processes such as telomere elongation by telomerase. In addition to duplex and higher-order nucleic acid structures, single-stranded polynucleotide chains have also been known to modulate key cellular processes. A well-known example is the poly(A) tail that is involved in RNA translation where it helps to cap the m-RNA and assists in its translation. Thus, targeting nucleic acids with a small molecule can lead to varied therapeutic results. The reports mentioned above were the first examples of higher-order DNA·RNA recognition by aminoglycosides and were later exploited in the development of high-affinity[23] and structure-selective nucleic acid binders.[5] Among all the aminoglycosides, neomycin (Figure 2a) has been reported to be the highest-affinity ligand in studies conducted on triplexes, hybrids,[10] and quadruplex nucleic acid structures.[24]

Studies have suggested that aminosugars bind to the major groove of nucleic acids, for example, the Watson−Hoogsteen groove of the T-A·T triplex,[25] or the major groove of the poly(rI)·poly(rC) duplex.[26] We have reported that aminoglycosides preferentially bind to nucleic acid structures that adopt A-like conformations.[27] However, with the developments in synthetic conjugates,[28] aminoglycoside conjugates can be developed to bind B-form DNA structures.[5,29] Neomycin−neomycin conjugates have been shown to bind B-DNA in the major groove with high affinities ($K_a = 10^8 \times M^{-1}$).[5] Similarly, by attaching aminosugars to other shape-selective ligands such as methidium carboxylic acid, subnanomolar binding to hybrid nucleic acids has been obtained.[30] The modification of aminoglycosides can be extended[31,32] with the conjugation of shape and sequence ligands such as intercalators and minor groove binders to achieve specificity and selectivity for targeted nucleic acids.[33,34] These nucleic acid structures all bind to aminosugars, yet do so with varying affinities. Additionally, all the aforementioned nucleic acid structures present a wide variation of shapes with varying major and minor groove widths. In this report, we explore the correlations between nucleic acid shape, as determined by major groove widths, and their affinities for an aminosugar (neomycin). In particular, the interaction of neomycin with different nucleic acid structures ranging from B-form to A-form, which include single, double, triple, and quadruple strands, is reported.

MATERIALS AND METHODS

Nucleic Acids and Aminoglycosides. All aminoglycosides were purchased from ICN Biomedicals Inc. (Solon, OH) and used without further purification. All the polynucleotides were purchased from GE Healthcare Amersham Biosciences (Piscataway, NJ). The concentrations of all the polymer solutions were determined spectrophotometrically using the following extinction coefficients (in units of moles of nucleotide or base pairs per liter per centimeter): ε_{264} = 8520 for poly(dT), ε_{260} = 6000 for poly(dA)·poly(dT), ε_{262} = 6600 for poly(dA-dT)·poly(dA-dT), ε_{254} = 8400 for poly(dG-dC)·poly(dG-dC), ε_{258} = 9800 for poly(A), ε_{260} = 9350 for poly(U), and ε_{274} = 7400 for poly(dC). $d(A_2G_{15}T_{15}T_2)$ was purchased from Integrated DNA Technologies (ε_{260} = 301200 per strand). 16S A-site rRNA was purchased from Dharmacon Inc. (Chicago, IL) and deprotected before being used (ε_{260} = 253300 per strand). Calf thymus DNA was purchased from Sigma (ε_{260} = 12824 per base pair). All other oligomers used were purchased from Eurofin MWG Operon (Huntsville, AL) and used without further purification.

Ultraviolet (UV) Spectroscopy. All UV experiments were conducted on a Cary 1E UV−vis spectrophotometer equipped with a temperature controller. Quartz cells with a 1 cm path length were used for all the experiments. All samples were heated at 95 °C for 5 min, cooled slowly to room temperature, and allowed to incubate for at least 16 h at 4 °C prior to being used. Absorbance versus temperature profiles were recorded at 260, 280, and 295 nm. For thermal denaturation experiments, the samples were heated from 5 to 95 °C at a rate of 0.2 °C/min followed by cooling to 10 °C at a rate of 5.0 °C/min. Data were recorded in 1 °C increments. For the determination of melting temperatures (T_m), the first derivative was used. For all the thermal denaturation experiments, DNA concentrations were 15−30 μM in base pair or 15−30 μM in base triplet.

Isothermal Titration Calorimetry (ITC). All isothermal calorimetric measurements were performed on a MicroCal VP-ITC (MicroCal, Inc., Northampton, MA) at 10 °C, except for temperature dependence experiments. In ITC studies, DNA concentrations were varied to obtain a reliable signal. In every titration, 5 or 10 μL aliquots of aminoglycoside solution were injected into a sample cell containing 1.42 mL of nucleic acid solution. The injection spacing was either 240 s or 300 s, the syringe rotation rate was 260 rpm, and the duration of each injection was 20 s. For each titration, a control experiment was performed by titrating the ligand into buffer. The resulting data were processed using Origin version 5.0. Each heat burst curve corresponds to a signal drug injection. Integrating the area under each heat curve yielded the heat released upon ligand injection. The corresponding heat of dilution was subtracted to yield the actual heat changes associated with ligand−nucleic acid binding.

dx.doi.org/10.1021/bi201077h | Biochemistry 2011, 50, 9088−9113

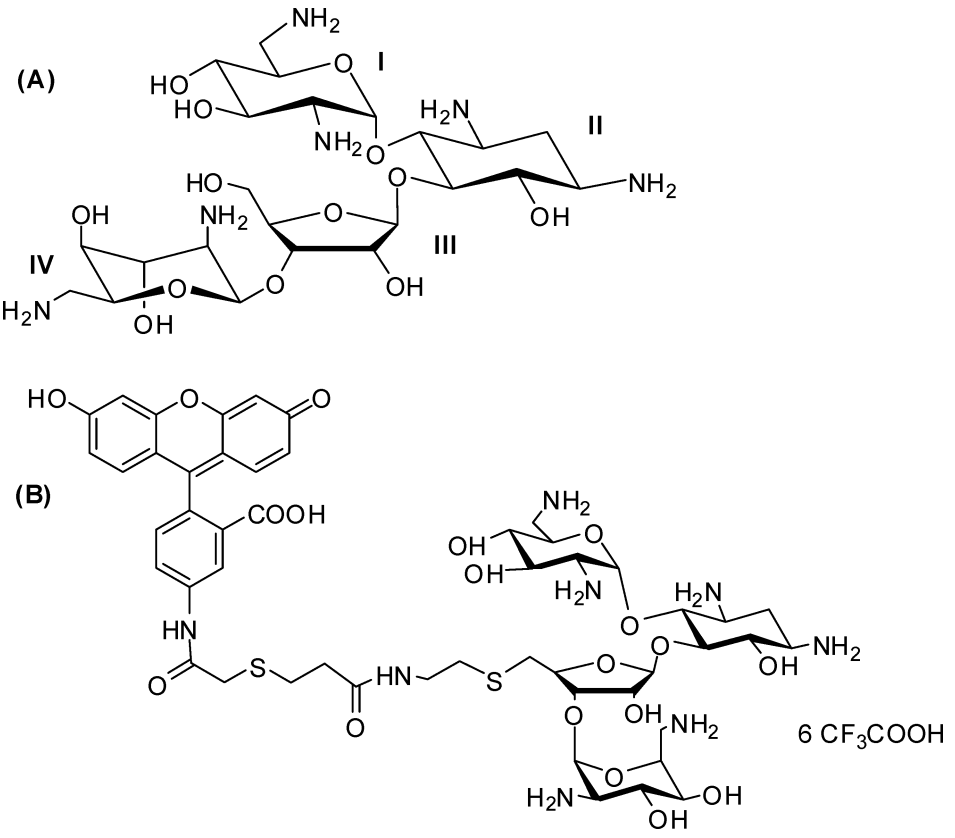

Figure 2. Chemical structure of (a) neomycin and (b) the fluorescein−neomycin conjugate.

Differential Scanning Calorimetry (DSC). The nucleic acid melting temperature and enthalpy changes in the absence of drug were obtained using a MicroCal VP-DSC (MicroCal, Inc.). The scan rate was 1 °C/min, and the operating temperature range was 5−110 °C. After each DSC experiment, a corresponding control experiment was conducted with only buffer in the sample cell. The corrected DSC profile was obtained by subtracting the control data from the sample data. The enthalpy changes for the melting of nucleic acids structures in the absence of ligand (ΔH_{HS}) were calculated by integrating the area under the heat capacity curves using Origin version 5.0.

Circular Dichroism (CD) Spectroscopy. All CD experiments were conducted at 20 °C on a JASCO J-810 spectrophotometer equipped with a thermoelectrically controlled cell holder. A quartz cell with a 1 cm path length was used in all CD studies. CD spectra were recorded as an average of three scans from 300 to 200 nm. In isothermal CD titration experiments, small aliquots of concentrated ligand solutions were added to nucleic acid solutions and allowed to equilibrate for at least 20 min prior to scanning.

Competition Dialysis. For each competition dialysis assay, 200 μL of different nucleic acids was placed in a MINI dialysis flotation device (Pierce Chemical Co.) and then dialyzed with 400 mL of 0.1 μM ligand in BPES buffer solution for 72 h at ambient temperature (20−22 °C). At the end of the experiment, 180 μL nucleic acid samples were carefully transferred to microfuge tubes and were taken to a final sodium dodecyl sulfate (SDS) concentration of 1% (w/v). Each mixture was allowed to equilibrate for 2 h. The concentration of ligand after dialysis was determined by fluorescence (Fluoromax-3, Jobin Yvon, Inc.). Appropriate corrections were made due to volume changes. The amount of bound drug was determined by the relationship $C_b = C_t - C_f$, where C_f is the concentration of the free ligand solution, C_t is total ligand concentration, and C_b is the concentration of the bound ligand. Data were plotted as a bar graph using Kaleidagraph (version 3.5, Synergy Software). A calibration curve was made to determine C_t and C_f.

Fluorescence Intercalator Displacement (FID) Assays. FID experiments were conducted on either a Photon Technology International (Lawrenceville, NJ) or TECAN-Genois 96 well plate reader. The FID experiments were performed at 20−22 °C with the polynucleotides and 10 °C with the oligonucleotides. In the 96-well plate experiments, a total volume of 200 μL was used. The total volume used in the fluorimeter experiments was 1.8 mL. For polynucleotides, the nucleic acid concentration used was 0.88 μM per base pair or triplet with a 1.24 μM thiazole orange (TO) concentration. For 30-mer oligonucleotides, the nucleic acid concentration was 1 μM per duplex or triplex with a 15 μM TO concentration. All experiments were performed in a buffer containing 10 mM sodium cacodylate, 100 mM NaCl, and 0.5 mM EDTA (pH 5.5 or 6.8). TO was excited at 504 nm, and the emission was recorded from 515 to 600 nm. The ligand concentration required to displace 50% of the bound fluorescent probe was determined from a dose−response curve and is expressed as AC_{50}.

ΔT_m Method. The following equation was used to calculate association constants at the corresponding melting temperatures at which the nucleic acid formed a complex with the ligand.[35]

$$\frac{1}{T_{mo}} - \frac{1}{T_m} = \frac{R}{n(\Delta H_{HS})} \ln(1 + K_{T_m} L) \quad (1)$$

dx.doi.org/10.1021/bi201077h | *Biochemistry* 2011, 50, 9088−9113

Scheme 1. Synthesis of F-neo Conjugate 4[a]

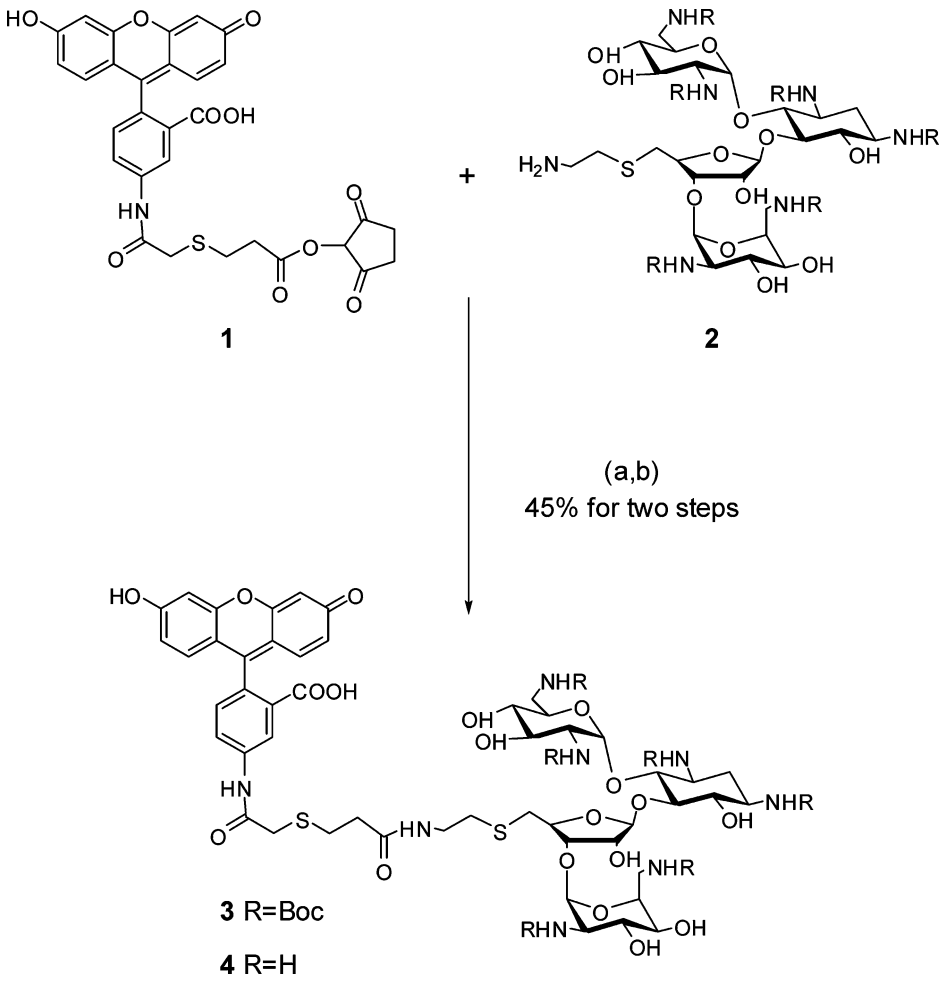

[a](a) Dimethylformamide (DMF), 4-dimethylaminopyridine (DMAP), room temperature; (b) TFA, dichloromethane (DCM), room temperature.

where T_{mo} is the melting temperature of ligand free nucleic acid, T_m is the melting temperature of ligand-bound nucleic acid, ΔH_{HS} is the enthalpy change corresponding to nucleic acid base pair melting in the absence of ligand (determined from a DSC measurement), L is the free ligand concentration at T_m (estimated by half of the total ligand concentration), and n is the binding site size determined by CD and fluororescence experiments. After the association constants at T_m had been determined, the integrated van't Hoff equation (eq 2) was used to calculate the association constants at 10 °C.[36]

$$K_{obs} = \frac{K_{T_m}}{e^{-\Delta H_{obs}/R(1/T_m - 1/T)} e^{\Delta C_p T(1/T_m - 1/T)} \left(\frac{T_m}{T}\right)^{\Delta C_p/R}} \quad (2)$$

where ΔH_{obs} is the observed enthalpy for binding of ligand to nucleic acid as derived from ITC excess site binding experiments at 10 °C, R is the gas constant, and ΔC_p is the heat capacity change determined from eq 3 by using binding enthalpies at various temperatures.

$$\Delta C_p = \frac{\partial H}{\partial T} \quad (3)$$

Synthesis of the Fluorescein–Neomycin Conjugate (F-neo) (4). The fluorescein–neomycin conjugate (**4**) was prepared by coupling an activated fluorescein ester (**1**) with neomycin amine (**2**) followed by deprotection of Boc groups using trifluoroacetic acid (TFA) (Scheme 1 and Figures S43 and S44 of the Supporting Information).

To a DMF solution (1 mL) of **1** (5 mg, 0.0086 mmol) and 4-dimethylaminopyridine (catalytic amount) was added **2** (10 mg, 0.0078 mmol) and the mixture stirred overnight at room temperature. The reaction mixture was concentrated under vacuum. Flash chromatography of the residue [8% (v/v) CH_3OH in CH_2Cl_2] yielded the Boc-protected F-neo conjugate as a yellow solid (10 mg): R_f 0.21 [10% (v/v) CH_3OH in CH_2Cl_2]. The product was then dissolved in CH_2Cl_2 (3 mL), and trifluoroacetic acid (0.5 mL) was added to it. The mixture was stirred at room temperature for 3 h. After the solvents had been removed under vacuum, the residue was dissolved in H_2O (2 mL) and extracted with dichloromethane (3 × 2 mL). The aqueous layer was concentrated under vacuum to yield the desired product (7 mg, 45% for two steps): UV–vis (H_2O) λ = 232, 455, 478 nm; ε (478 nm) = 13260 M^{-1} cm^{-1}; ^1H NMR (500 MHz, D_2O) δ 8.34 (s, br, 1H), 7.86 (m, 2H), 7.47–7.45 (d, J = 9.3 Hz, 2H), 7.33- 7.32 (d, J = 8.20 Hz, 1H), 7.23 (s, br, 1H), 7.07–7.05 (d, J = 9.36 Hz, 1H), 6.74–6.73 (d, J = 6.73 Hz, 1H), 5.96–5.94 (m, 1H) (ring I-1′), 5.32–5.29 (br, 2H) (contains ring III-1″), 5.19 (s, br, 1H) (ring IV-1‴), 4.33–4.17

dx.doi.org/10.1021/bi201077h | Biochemistry 2011, 50, 9088–9113

Table 1. AC_{50} Values Obtained from the FID Assay of the Polynucleotides[a]

	AC_{50} (μM)			
nucleic acid	neomycin	paromomycin	ribostamycin	neamine
poly(rA)·poly(rU)	0.02 ± 0.01	0.13 ± 0.02	0.32 ± 0.08	1.2 ± 0.2
poly(rA)·2poly(rU)	0.09 ± 0.01	0.45 ± 0.08	2.30 ± 0.60	7.40 ± 0.30
poly(dA)·poly(rU)	1.2 ± 0.2	1.5 ± 0.4	10 ± 3	119.00[b]
poly(rA)·poly(dT)	1.6 ± 0.2	40[b]	60[b]	234[b]
poly(dA)·2poly(dT)	2.4[b]	22.4[b]	37.2[b]	355[b]
poly(dA-dT)$_2$	5.1 ± 0.2	57 ± 3	239[b]	609 ± 17

[a]See Materials and Methods for experimental conditions. [b]Data obtained from FID titration experiments in a 3.0 mL quartz cell . All other experiments were conducted in a 96-well plate.

(m, 4H) (contains ring III-2‴, ring IV-3″), 4.01−3.97 (t, J = 9.67 Hz, 1H), 3.93−3.89 (t, J = 10.3 Hz, 1H), 3.83−3.78 (m, 2H), 3.71 (s, br, 1H), 3.61−3.57 (t, J = 9.89 Hz, 1H), 3.49−3.11 (m, 16H) (contains ring IV-2‴, ring II 1′, ring II-3′), 3.07−2.99 (m, 3H), 2.87−2.84 (m, 2H), 2.73−2.61 (m, 2H), 2.55−2.53 (t, J = 6.52 Hz, 2H), 2.39−2.37 (br, 1H) (ring II, 2 equiv), 1.83−1.76 (m, 1H) (ring II-2$_{ax}$); MS (MALDI-TOF) calcd m/z for $C_{50}H_{68}N_8O_{19}S_2Na$ 1171.22, found 1171.86.

Docking Studies. All dockings were performed as blind dockings using Autodock Vina 1.0.[37] Docking was performed using an "exhaustiveness" value of 12. All other parameters were default values. All rotatable bonds within the ligand were allowed to rotate freely, and the receptor was kept rigid. The Protein Data Bank was used to download the nucleic acid receptors (entries are listed with sequences in Tables S1−S3 of the Supporting Information). All ligand structures were created using Discovery Studio Visualizer 2.5 and then brought to their energetically minimized structures with Vega ZZ[38] utilizing a conjugate gradient method with an SP4 force field. Autodock Tools version 1.5.4[39] was used to convert the ligand and receptor molecules to the proper file formats for AutoDock Vina docking.

RESULTS

Fluorescence Intercalator Displacement (FID). FID assays have been shown to offer a means for qualitative comparison of relative binding affinities.[40] Two separate but comparable FID methods were employed; fluorescence titrations and 96-well plate reader fluorescence titrations performed in triplicate. In both methods, thiazole orange (TO) was used as the intercalator that was displaced by the ligand. In addition to neomycin, three other aminoglycosides (paromomycin, ribostamycin, and neamine) were screened to assess the relative binding of these structurally similar ligands. In addition to polynucleotides, 30-mer oligonucleotides were also studied with neomycin. The results are summarized in Tables 1 and 2.

Table 2. AC_{50} Values Obtained from the FID Assays of 30-mer Oligonucleotides[a]

nucleic acid	neomycin AC_{50} (μM)
rA$_{30}$·rU$_{30}$	0.68
rA$_{30}$·2rU$_{30}$	2.2
dA$_{30}$·rU$_{30}$	6.6
rA$_{30}$·dT$_{30}$	7.9
dA$_{30}$·dT$_{30}$	8.9
dA$_{30}$·2dT$_{30}$	53.7[b]

[a]See Materials and Methods for experimental conditions. [b]The AC_{50} value was obtained with additional 150 mM KCl salt to ensure stable triplex formation.

The AC_{50} values represent the ligand concentrations required to displace 50% of the bound fluorescent probe and are derived from sigmoidal fits for the fluorescence titration curves (Tables 1 and 2 and Figures S1−S8 of the Supporting Information). Lower AC_{50} values generally represent higher affinities as less ligand is required to displace the bound intercalator. The 30-mer sequences generally followed the trend established in Table 1 with one exception, the dA$_{30}$·2dT$_{30}$ triplex, which had an AC_{50} value substantially higher than those of the other complexes because of the higher salt concentration needed for formation (also see Competition Dialysis). Overall, the order of the AC_{50} values for interactions of neomycin with nucleic acids was as follows: poly(rA)·poly(rU) ∼ poly(rA)·2poly(rU) < poly(dA)·poly(rU) < poly(rA)·poly(dT) < poly(dA)·2poly(dT) < poly(dA-dT)$_2$. In terms of individual interactions of aminoglycosides with the nucleic acids, neomycin exhibited the lowest AC_{50} value followed by paromomycin, ribostamycin, and neamine.

Competition Dialysis. We have previously reported that in addition to the 16S A-site rRNA, aminoglycosides bind to nucleic acids that adopt A-form structures.[21,27] To explore aminoglycoside structure selectivity, we used competition dialysis as a nucleic acid screening technique[41] to illustrate the binding of neomycin to different nucleic acid structures. Previous inquiries have reported the use of an acridine derivative to follow the nucleic acid selectivity in the competition dialysis assay.[42] Acridine, however, binds to several nucleic acids and therefore perturbs the selectivity of the free aminoglycoside. We herein report the competition dialysis studies using a fluorescein−neomycin conjugate (F-neo) (Figure 2b). As a control, binding of fluorescein to nucleic acids was investigated in the competition dialysis assay and showed negligible binding.

As shown in panels a, c, and e of Figure 3, comparative binding of F-neo to 14 different nucleic acid structures was examined, including single-strand nucleic acids [poly(dT), poly(A), and poly(U)], duplexes [poly(dA)·poly(dT), poly(rA)·poly(dT), poly(rA)·poly(rU), poly(dA)·poly(rU), poly(dG)·poly(dC), and calf thymus DNA], triplexes [poly(dA)·2poly(dT) and poly(rA)·2poly(rU)], an i-motif [poly(dC)], and 16S A-site rRNA. The amount of F-neo bound to each nucleic acid is shown as a bar graph. Because all nucleic acids are dialyzed simultaneously in the same ligand solution, the amount of bound F-neo is directly proportional to its affinity for each nucleic acid.[41]

Figure 3 suggests the following conclusions. First, F-neo prefers to bind to 16S A-site rRNA yielding a bound ligand concentrations of 85 nM in 100 mM Na^+, 50 nM in 150 mM

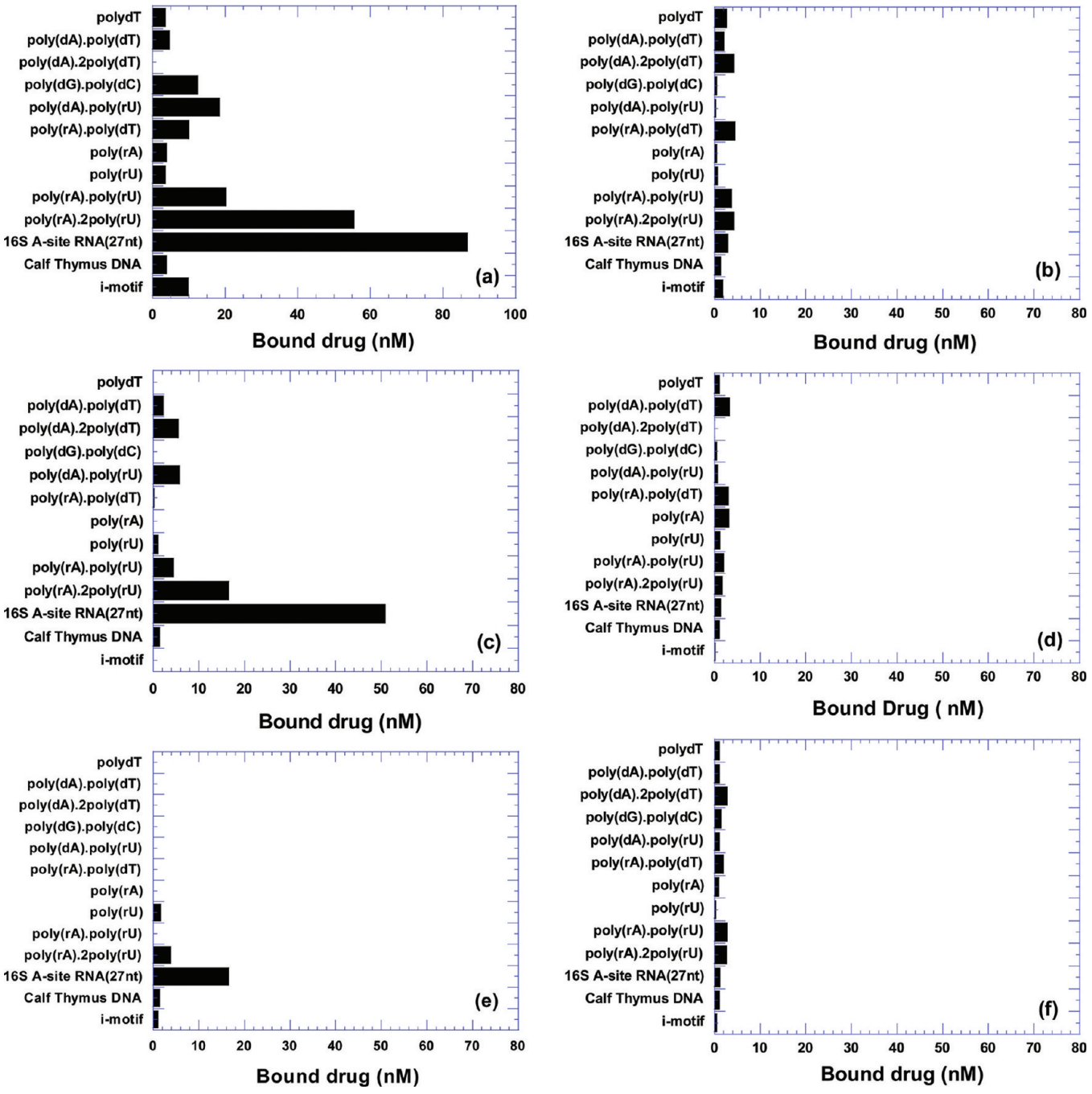

Figure 3. (a, c, and e) Competition dialysis results for the fluorescein−neomycin conjugate with various nucleic acids at (a) 100, (c) 150, and (e) 200 mM Na^+. (b, d, and f) Competition dialysis results of fluorescein with various nucleic acids at (b) 100, (d) 150, and (f) 200 mM Na^+. Different nucleic acids (200 μL, 7.5 μM per monomeric unit of each polymer) were dialyzed for 72 h with 400 mL of 100 nM ligand in 6 mM Na_2HPO_4, 2 mM NaH_2PO_4, 1 mM Na_2EDTA (pH 7.0), and various Na^+ concentrations as indicated.

Na^+, and 15 nM in 200 mM Na^+. Binding to the RNA triplex poly(rA)·2poly(rU) is comparable to binding to A-site rRNA under low-salt conditions, with 60, 20, and 5 nM bound F-neo in 100, 150, and 200 mM Na^+, respectively. F-neo also shows significant binding to RNA duplex poly(rA)·poly(rU), DNA triplex poly(dA)·2poly(dT), and hybrid duplex poly(dA)·poly(rU) with approximately 10−20 nM bound drug under these salt conditions. However, F-neo exhibits moderate to very weak binding with DNA duplex poly(dA)·poly(dT), hybrid duplex poly(rA)·poly(dT), calf thymus DNA, i-motif DNA, and all single-stranded nucleic acids studied here.

Second, the binding of F-neo to nucleic acids is affected by the salt concentration. As the Na^+ concentration increases from 100 to 200 mM, the amount of bound neomycin decreases approximately 4−5 times for each nucleic acid structure. These results are also consistent with the thermodynamic studies of neomycin−nucleic acid interaction, as discussed below (Table 4).

Third, fluorescein itself shows little binding affinity for any nucleic acid under all three salt conditions as shown in Figure 3b,d,f. The concentration of bound fluorescein is <4 nM under

dx.doi.org/10.1021/bi201077h | *Biochemistry* 2011, 50, 9088−9113

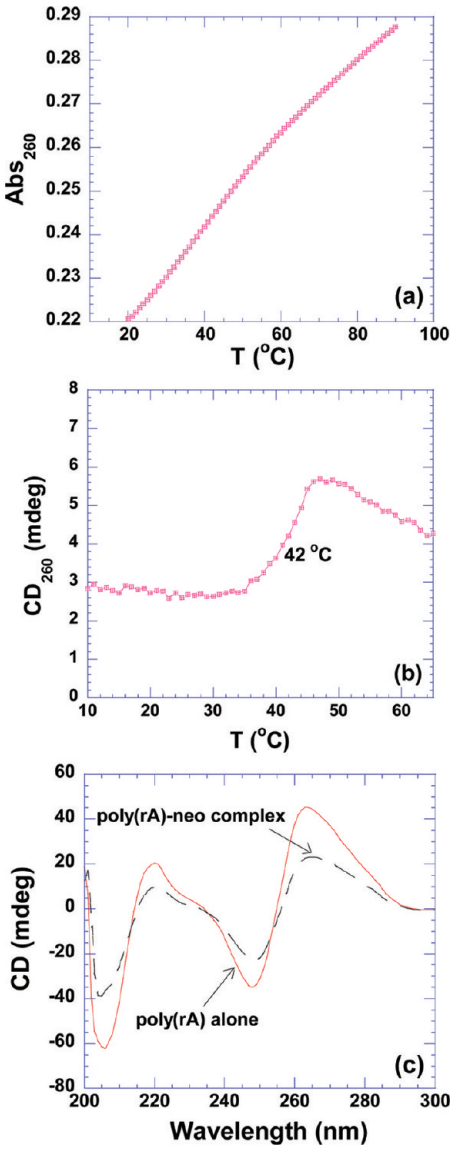

Figure 4. (a) UV thermal denaturation profile of poly(rA). (b) CD thermal denaturation profile of poly(rA) (20 μM/strand) in the presence of neomycin at an r_{bd} of 4. (c) CD scans of poly(rA) (75 μM/strand) in the absence and presence of neomycin. The experiments were conducted in 10 mM sodium cacodylate, 0.5 mM EDTA, and 100 mM NaCl (pH 6.8).

all three salt conditions, suggesting fluorescein's contribution in F-neo conjugate binding is insignificant.

Fourth, the counterintuitive and surprising absence of binding of F-neo to poly(dA)·2poly(dT) under 100 mM Na^+ can be explained by the nonformation of the DNA triplex at this salt concentration at ambient temperatures (~22 °C). As the Na^+ concentration is increased to 150 mM, triplex formation is favored and ligand binding is observed.

Competition dialysis reveals that F-neo binds the natural target 16S A-site rRNA and also shows comparable binding to RNA triplex. Analysis of the nucleic acid structures that are favored by neomycin suggests that they all display features characteristic of the A-form conformation. The hybrid duplex, especially poly(dA)·poly(rU), exhibits a conformation that is intermediate between the A- and B-forms, but more like A-form.[43] The low level of bound drug observed for poly(rA)·poly(dT) can be attributed to the fact that this hybrid can exist in the B-form.[43,44] In addition, GC-rich sequences are well-known to adopt an A-like conformation in aqueous solution.[45] Highly ordered nucleic acid structures such as the G-quadruplex and triplex also adopt a conformation exhibiting some A-form features[46] as indicated by a strong band in the vicinity of either 260 or 205 nm in their CD spectrum. More importantly, the size of their major grooves lies intermediate between the widths and depths of an A-form major groove and a B-form major groove.

Thermodynamic Study of Nucleic Acid–Neomycin Interactions. *Polyadenylic Acid [poly(rA)]. pH 5.5.* A poly(rA)·poly(rA) duplex has been shown to form at pH 5.5.[47] CD titrations of the duplex with neomycin at pH 5.5 show large positive bands at 260 nm and small negative bands at 240 nm,[47] indicating the presence of the poly(rA)·poly(rA) duplex. The rotational symmetry of the A-A base pair causes this duplex to form identical grooves.[43] Further, the RNA duplex has been shown to undergo significant stabilization upon binding with neomycin[47] with no overall conformational change and a 6.5 bp/drug binding site size (approximately one helical turn of 8 bp bound to each ligand[47]). Neomycin binds to this A-form RNA structure with a high binding affinity (K_a) of $(1.7 \pm 0.2) \times 10^7$ M^{-1} (Table 4).

pH 6.8. Poly(rA) exists as a single strand at pH 6.8. The single-stranded poly(rA) also undergoes a broad denaturation with an increase in temperature, indicating a structural transition from a stacked helix to a random coil as shown in Figure 4a. In the presence of neomycin, the thermal denaturation results reveal that the transition becomes sharper, as shown in the CD melting profile (Figure 4b). Here, a positive transition for the poly(rA)–neomycin complex associated with an increase in temperature is clearly observed. These observations indicate a conformational change in poly(rA) upon neomycin binding. To investigate the neomycin-induced poly(rA) conformation, we conducted a CD study. The CD spectrum of poly(rA) in the absence of neomycin at pH 6.8 shows a positive band around 265 and 220 nm and a strong negative band at 250 nm, characteristic of single-stranded poly(rA) (Figure 4c).[48] When neomycin is added to the poly(rA) solution, the intensities of the CD bands decrease, and little red or blue shift is observed (Figure 4c). The neomycin-induced CD spectrum at pH 6.8 is clearly different from that obtained at pH 5.5, indicating significant structural differences.

Small molecules, such as protoberberine alkaloids berberine,[48] palmatine,[49] and coralyne,[50] have been shown to bind strongly to single-stranded poly(rA). The binding mode for these ligands is hypothesized to be a partial intercalation in which the ligand molecule is inserted between neighboring adenine bases through the stacking of the ligand between the bases on the chain.[48] The binding of neomycin to poly(rA) found here generates a CD spectrum similar to those of berberine and palmatine, suggesting the involvement of a similar RNA structure. However, additional structural studies will be needed to confirm these analyses and understand the poly(rA) conformation induced by neomycin.

Polyuridylic Acid [poly(rU)]. RNA homopolymer poly(U) does not show a clear melting transition in the temperature range studied (10–75 °C) at either high or low pH (Figure S9 of the Supporting Information). It has been reported that poly(rU) does not possess any specific structure at ambient temperatures, indicating a lack of stacking interaction between the uridine bases, thereby leading to a random-coil con-

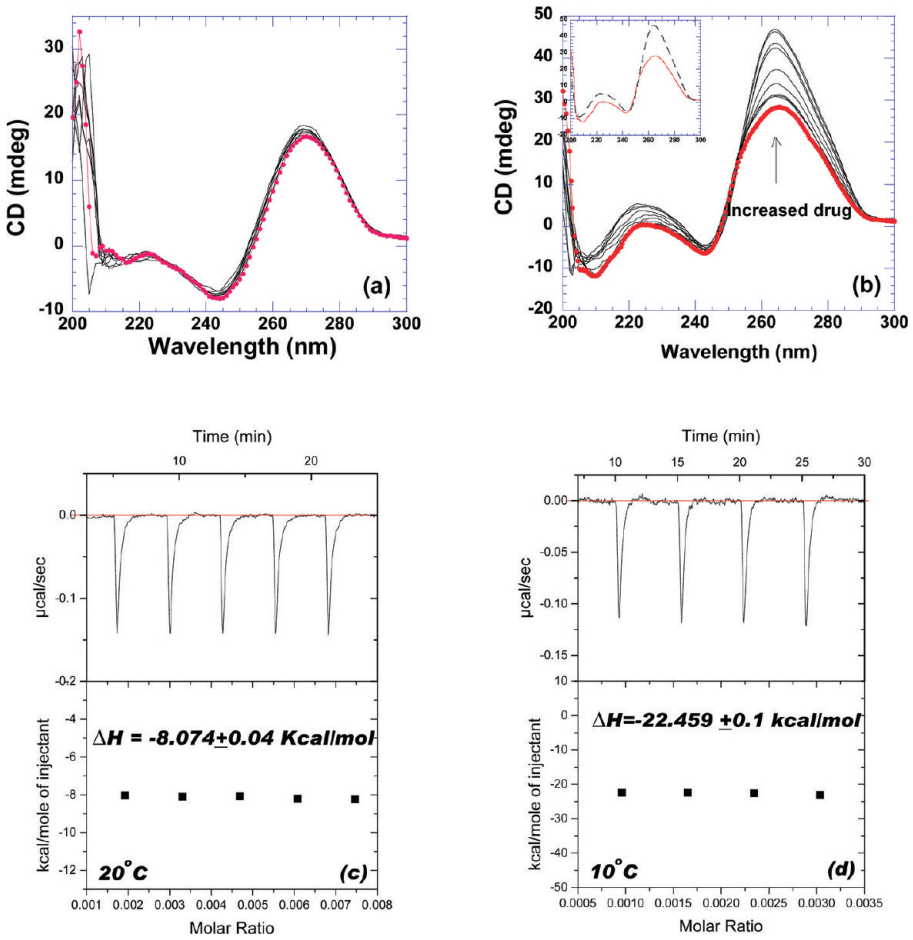

Figure 5. CD titration of neomycin into poly(rU) (100 μM/strand) at (a) 59 and (b) 20 °C. The filled circles show data of the RNA by itself. The inset in panel b shows the CD spectra of RNA alone (—) and the ligand-saturated complex (---). ITC titration of neomycin with poly(rU) (200 μM/strand) at (c) 20 and (d) 10 °C . The experiments were conducted in 10 mM sodium cacodylate, 0.5 mM EDTA, and 100 mM NaCl (pH 6.8).

formation.[51] However, poly(rU) has been found to exhibit a secondary structure, an antiparallel double helix, at low temperatures.[52] This structure is reported to adopt an A-form conformation.[53] The stability of this duplex is quite low, exhibiting a melting temperature of ∼5 °C. Counterions and polyamines such as spermine have been shown to stabilize this poly(rU)·poly(rU) duplex significantly.[54]

A CD scan was taken at high temperatures for randomly structured poly(rU) (Figure 5a). A strong positive band at 270 nm, a negative band at 243 nm, and a very strong positive band at 203 nm were observed. These peaks are considered to be characteristic CD peaks for single-stranded poly(rU). The CD scan at 20 °C shows a 5 nm blue shift of the 270 nm band and the development of a new negative peak around 210 nm (Figure 5b), indicating the formation of a secondary structure. This secondary structure, the antiparallel double-stranded poly(rU), shows unexpectedly high binding enthalpies when it forms a complex with neomycin [−8.1 ± 0.4 and −22.5 ± 0.1 kcal/mol (Figure 5c,d)]. In contrast to those of all other nucleic acids investigated, this observed binding enthalpy increased in magnitude as the temperature decreased (Figure 5d). A likely reason for this observation is the fact that neomycin favors double-stranded poly(rU) and has no effect on single-stranded poly(rU). The significantly lower binding enthalpy at 20 °C can be attributed to the decreased number of poly(rU) duplex species in solution. Furthermore, addition of neomycin to poly(rU) at 20 °C increased the magnitude of the positive CD signal and induced a blue shift of bands at 270 and 210 nm (Figure 5b). As for the poly(rA) system, the ΔT_m method is not applicable here in calculating the binding constant of neomycin bound to poly(rU) at pH 5.5 or 6.8 because of the difficulties in experimentally determining the melting temperature.

AT-Rich Duplexes Poly(dA)·Poly(dT) and Poly(dA-dT)·Poly(dA-dT). The conformations of polynucleotide AT-rich duplexes poly(dA-dT)·poly(dA-dT) and poly(dA)·poly(dT) are B- and B*-form DNA, respectively, containing a narrow minor groove and a wide and shallow major groove. The two polymers possess differing physical properties. For example, the melting temperature of poly(dA)·poly(dT) (AT duplex, 69.3 °C) is ∼8 °C higher than that of poly(dA-dT)·poly(dA-dT) (alternating AT duplex, 61.7 °C) (Table 3 and Figures S10 and S11 of the Supporting Information). In addition, the disproportionation of the poly(dA)·poly(dT) duplex to a poly(dA)·2poly(dT) triplex and the single-stranded poly(dA) is observed at low pH, similar to the disproportionation of the poly(rA)·poly(rU) duplex into a triplex and single strands.[43]

pH 5.5. Disproportionation of poly(dA)·poly(dT) in the presence of neomycin was observed at pH 5.5 (Figure 6a). Beginning at 30 °C, the absorbance of the solution gradually decreased, indicating the rearrangement of poly(dA) and poly(dT). This rearrangement was complete at 80 °C, and the poly(dA)·2poly(dT) that formed after disproportionation denatured directly from a triplex to single strands at 91 °C.

dx.doi.org/10.1021/bi201077h | *Biochemistry* 2011, 50, 9088–9113

Table 3. Thermodynamic Profiles of the Interaction of Neomycin with a Variety of Nucleic Acids in 10 mM Sodium Cacodylate, 0.5 mM EDTA, and 100 mM NaCl (pH 6.8)

	ΔH_{wc} (kcal/mol)	T_{mo} (°C)	T_m (°C)	ΔT (°C)	n	$\Delta H_{10\ °C}$ (kcal/mol)	$\Delta H_{20\ °C}$ (kcal/mol)	$\Delta H_{30\ °C}$ (kcal/mol)	ΔC_p (cal mol^{-1} K^{-1})
poly(rA)	–	–	42.0	–	4.0	–	–	–	–
poly(rU)	–	<10	20.0	–	8.5	−22.5 ± 0.1	−8.1 ± 0.1	–	–
poly(dA-dT)·poly(dA-dT)	5.17	61.7	62.5	0.5	7.0	−3.4 ± 0.1	−3.7 ± 0.2	–	−26 ± 24
poly(dG-dC)·poly(dG-dC)	6.10	111.7	112.7	1.0	6.0	−2.7 ± 0.1	−3.0 ± 0.1	–	−28 ± 22
poly(dA)·poly(dT)	4.04	69.3	69.7	0.4	9.0	−7.2 ± 0.1	−7.7 ± 0.3	–	−58 ± 25
calf thymus DNA	10.25	84.4	85.0	0.6	6.0	−3.7 ± 0.1	−5.0 ± 0.1	–	−120 ± 16
i-motif	4.25	50.0	53.5	3.5	4.0	−6.4 ± 0.2	−7.9 ± 0.1	–	−151 ± 32
poly(rA)·poly(dT)	9.21	65.2	67.3	2.1	8.0	−2.5 ± 0.1	−3.9 ± 0.1	−5.7 ± 0.1	−159 ± 50
$d(A_2G_{15}C_{15}T_2)_2$	3.41	93.8	95.2	1.4	10.0	−7.2 ± 0.1	−9.5 ± 0.2	−11.9 ± 0.1	−235 ± 10
poly(rA)·2poly(rU)	12.21 (3 > 1)	59.0	–	–	8.5	−4.6 ± 0.2	−7.0 ± 0.1	−9.4 ± 0.1	−238 ± 22
poly(dA)·2poly(dT)	1.00	23.4	50.0	26.6	7.0	−6.6 ± 0.1 (10 °C)	−7.9 ± 0.1 (15 °C)	−8.7 ± 0.1 (18 °C)	−264 ± 23
poly(rA)·poly(rU)	6.75	59.0	73.1	14.1	7.0	−4.2 ± 0.1	−7.6 ± 0.1	−9.8 ± 0.1	−279 ± 11
poly(dA)·poly(rU)	5.3	48.4	65.2	16.8	6.0	−2.8 ± 0.1	−6.3 ± 0.1	−9.0 ± 0.1	−311 ± 15
16S A-site RNA	78.8	71.8	75.4	3.6	1.0	−9.7 ± 0.1	−13.0 ± 0.1	−16.7 ± 0.1	−350 ± 20

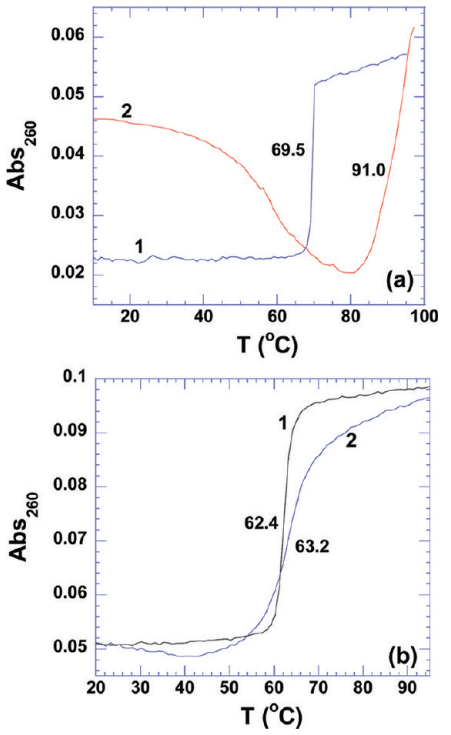

Figure 6. (a) UV thermal denaturation profiles of poly(dA)·poly(dT) in the absence (1) and presence (2) of neomycin at an r_{bd} of 5. (b) UV thermal denaturation of poly(dA-dT)·poly(dA-dT) in the absence (1) and presence (2) of neomycin at an r_{bd} of 5. The experiments were conducted in 10 mM sodium cacodylate, 0.5 mM EDTA, and 100 mM NaCl (pH 5.5).

Because of the formation of poly(dA)·2poly(dT) under this condition, the stabilization of poly(dA)·poly(dT) by neomycin cannot be evaluated, thus preventing the calculation of the binding constant using the ΔT_m method.

Unlike poly(dA)·poly(dT), alternating AT duplex poly(dA-dT)·poly(dA-dT) does not disproportionate into a triplex (Figure S12 of the Supporting Information). The thermal stabilization upon binding of neomycin to poly(dA-dT)·poly(dA-dT) was, however, observed to be very small ($\Delta T_m \sim 1$ °C) (Figure 6b). The heat capacity change derived from ITC titration was observed to be -16 ± 10 cal mol^{-1} K^{-1} (Table 4), indicating almost no solvent-accessible surface area change upon binding. Using this small change in denaturation temperature, the association constant of neomycin binding to poly(dA-dT)·poly(dA-dT) was estimated to be $(8.9 \pm 0.1) \times 10^4$ M^{-1} (Table 4). Further analysis of the thermodynamic data showed that 74% of the driving force of binding was entropy-driven (Figure 23).

pH 6.8. As expected, both poly(dA-dT)·poly(dA-dT) and poly(dA)·poly(dT) exhibit higher binding enthalpies at pH 6.8 [-3.7 ± 0.2 and -7.7 ± 0.3 kcal/mol, respectively (Table 3 and Figure 7)]. In addition, both duplexes show small heat capacity changes upon neomycin binding [-26 ± 24 cal mol^{-1} K^{-1} for poly(dA-dT)·poly(dA-dT) and -58 ± 25 cal mol^{-1} K^{-1} for poly(dA)·poly(dT) (Table 3)]. Thermal denaturation experiments revealed a negligible change ($\Delta T_m \sim 0.5$ °C) in the melting temperature upon neomycin binding. The binding enthalpy obtained at pH 6.8 includes the heat of protonation of amino groups upon formation of a complex of neomycin and the nucleic acid. Therefore, all association constants reported using the ΔT_m method in this article were obtained at pH 5.5.

Table 4. Thermodynamic Profiles of the Interaction of Neomycin with a Variety of Nucleic Acids in 10 mM Sodium Cacodylate, 0.5 mM EDTA, and 100 mM NaCl (pH 5.5)

	ΔH_{wc} (kcal/mol)	T_{mo} (°C)	T_m (°C)	ΔT (°C)	n	ΔH_{T1} (kcal/mol)	ΔH_{T2} (kcal/mol)	ΔC_p (cal mol^{-1} K^{-1})	$K_{T(20\ °C)}$ (M^{-1})
poly(dA-dT)·poly(dA-dT)	3.90	62.4	63.2	0.8	7.3	−2.1 ± 0.1 (40 °C)	−2.3 ± 0.1 (53 °C)	−16 ± 10	$(8.9 \pm 0.1) \times 10^4$
poly(dA)·2poly(dT)	1.21	23.5	31.0	7.5	6.0	−0.6 ± 0.3 (5 °C)	−3.2 ± 0.5 (15 °C)	−264 ± 30	$(2.4 \pm 0.1) \times 10^5$
poly(rA)·poly(dT)	7.12	64.1	67.5	3.4	8.0	−4.5 ± 0.1 (35 °C)	−5.0 ± 0.2 (45 °C)	−50 ± 20	$(3.4 \pm 0.4) \times 10^6$
poly(dA)·poly(rU)	3.84	43.6	65.5	21.9	6.5	3.6 ± 0.1 (15 °C)	2.8 ± 0.1 (20 °C)	−160 ± 18	$(9.4 \pm 0.1) \times 10^6$
$d(A_2G_{15}C_{15}T_2)_2$[a]	3.00	93.7	101.1	7.4	10.0	−0.7 ± 0.1 (20 °C)	−2.7 ± 0.1 (30 °C)	−173 ± 23	$(1.8 \pm 0.6) \times 10^7$
poly(rA-rA)	4.05	44.0	61.5	17.5	6.5	−1.8 ± 0.1 (5 °C)	−2.1 ± 0.1 (10 °C)	−60 ± 25	$(1.7 \pm 0.2) \times 10^7$
poly(rA)·poly(rU)	6.34	53.4	64.7	11.3	8.0	1.7 ± 0.1 (15 °C)	−0.7 ± 0.1 (25 °C)	−245 ± 7	$(2.9 \pm 0.1) \times 10^7$
poly(rA)·2poly(rU)	1.40	45.5	–	–	–	2.42 ± 0.02 (15 °C)	0.02 ± 0.01 (25 °C)	−240 ± 3	–
16S A-site RNA[a]	96.6[b]	70.8	77.0	6.2	1.0	−0.9 ± 0.1 (10 °C)	−2.4 ± 0.1 (20 °C)	−151 ± 12	$(8.7 \pm 0.9) \times 10^7$

[a]Data obtained from ITC titration experiments. [b]The melting enthalpy corresponds to the melting of a molecule of the nucleic acid.

GC-Rich Duplexes Poly(dG)·Poly(dC), $d(A_2G_{15}C_{15}T_2)_2$, and Poly(dG-dC)·Poly(dG-dC). GC tract DNA can adopt either an A-form or a B-form conformation, depending on the guanine-guanine base stacking. The poly(dG)·poly(dC) fiber is known to exhibit the A-form conformation,[55,56] but in the aqueous solution and at a low salt concentration (30 mM NaCl), poly(dG)·poly(dC) was also found to adopt a B-form conformation.[57] This B-form conformation of poly(dG)·poly(dC) can be converted to the A-form by changing the salt concentrations.[57] The A-form can be also be significantly stabilized by C5 methylation.[57] However, the study of long runs of $G_n{\cdot}C_n$ sequence can be problematic because of aggregation and the susceptibility of base pair slippage.[58,59] Moreover, multiple structures may coexist in the 1:1 poly(dG)/poly(dC) aqueous solution.[60] For example at pH 8.0, both the 2poly(dG)·poly(dC) triplex and the poly(dG)·poly(dC) duplex were found to coexist in solution.[60] As shown in Figure 8a, the DSC melting profile of poly(dG)·poly(dC) exhibits two peaks, one at ∼93.2 °C and the other at ∼102.7 °C at pH 6.8. This structure of poly(dG)·poly(dC) is affected by ionic strength, resulting in only one transition at 96.2 °C in 150 mM KCl (data not shown). More strikingly, the structure of the original poly(dG)·poly(dC) is not re-formed after renaturation. The newly formed structure melts at approximately 60 °C (data not shown). The addition of neomycin to this GC-rich duplex shifts to the red the positive peak at 257 nm and induces a strong negative peak at 210 nm, as well (Figure 8b). This change in the CD spectrum suggests induction of an A-form-like conformation. However, the spectrum also displays two shoulders at 257 and 290 nm, which negates the existence of a pure A-form conformation in solution (Figure 8b). This heterogeneous composition of the poly(dG)·poly(dC) aqueous solution prevented us from obtaining thermodynamic data upon neomycin interaction. Therefore, a GC-rich oligomer, $d(A_2G_{15}C_{15}T_2)_2$, has been used as a model for poly(dG)·poly(dC) and is discussed in the next section.

$d(A_2G_{15}C_{15}T_2)_2$. pH 5.5. Although GC tract sequences are known to have a propensity for A-form structures, an absolute A-form structure (as evidenced by CD spectroscopy) was not observed for this duplex under the conditions studied (Figure 9a). However, addition of neomycin converts the self-complementary $d(A_2G_{15}C_{15}T_2)_2$ duplex to the A-form, observed as a predominant CD band at 270 nm (Figure 9a), consistent with previous reports.[61] The structural basis for the B-form to A-form transition can be explained by the relative proximity of two negatively charged sugar−phosphate backbones along the major groove of the A-form conformation that can be neutralized by the positively changed amino groups present on these ligands.[61]

Neomycin has a greater stabilizing effect on the $d(A_2G_{15}C_{15}T_2)_2$ duplex at pH 5.5 than at pH 6.8 [$\Delta T_m \sim 7$ °C at an r_{bd} of 10 and pH 5.5 (Table 4 and Figure 9b)] compared with a <2 °C increase at pH 6.8 (Table 3 and Figure 9c). However, the ITC-derived heat capacity change [−173 ± 23 cal mol^{-1} K^{-1} (Table 4 and Figure S13 of the Supporting Information)] is significant at such a low pH value, which implies enhanced binding due to the removal of a large amount of nonpolar surface area. A direct ITC titration led to an association constant for binding of neomycin to the $d(A_2G_{15}C_{15}T_2)_2$ duplex of $(1.8 \pm 0.6) \times 10^7$ M^{-1} at pH 5.5 (Table 4). A breakdown of binding energetics revealed a large contribution from entropy (∼92%) for this interaction at low pH (Figure 23).

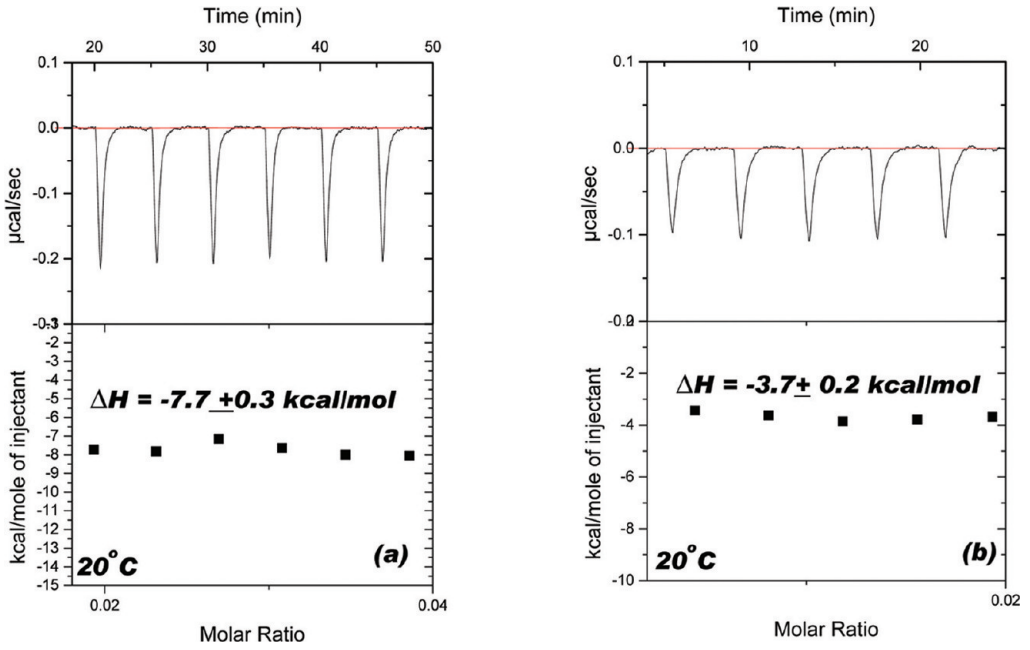

Figure 7. ITC titration of neomycin into (a) poly(dA)·poly(dT) (150 μM/bp) or (b) poly(dA-dT)·poly(dA-dT) at 20 °C (150 μM/bp). The experiments were conducted in 10 mM sodium cacodylate, 0.5 mM EDTA, and 100 mM NaCl (pH 6.8).

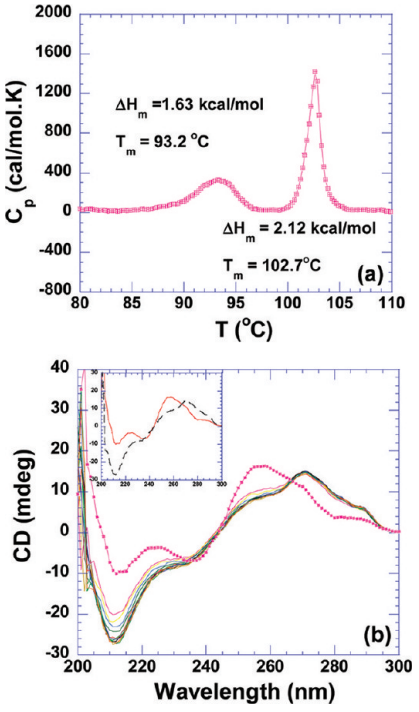

Figure 8. (a) DSC melting profile of poly(dG)·poly(dC) (100 μM/bp) at pH 6.8. (b) CD scans of the titration of neomycin with poly(dG)·poly(dC) (75 μM/bp) at pH 6.8. The experiments were conducted in 10 mM sodium cacodylate, 0.5 mM EDTA, and 100 mM NaCl.

pH 6.8. The conformation of the $d(A_2G_{15}C_{15}T_2)_2$ duplex at pH 6.8 was observed to be similar to the conformation observed at pH 5.5 as seen from the CD spectra (Figure S14 of the Supporting Information). However, the heat capacity change observed at pH 6.8 [-235 ± 10 cal mol^{-1} K^{-1} (Table 3, Figure 9d, and Figure S15 of the Supporting Information)] is larger than that obtained at pH 5.5. In addition to the change in solution electrostatics, the heats of amino group protonation of neomycin likely contribute to the difference in the heats of binding and heat capacities.

Poly(dG-dC)·Poly(dG-dC). Alternating GC sequence poly(dG-dC)·poly(dG-dC) was also studied and exhibited conformational features different from those of $G_n{\cdot}C_n$ tract sequences. As seen in Figure 10a, poly(dG-dC)·poly(dG-dC) displays a negative band at 247 nm and two positive overlapping bands at 265 and 285 nm. This can be identified as B-form base stacking through a comparison with its related canonical B-form structure, d(GCGCGCGC), while the peak at 265 nm corresponds to A-form base stacking.[45] Although poly(dG-dC)·poly(dG-dC) exhibits some features of the A-form structure, overall it is still regarded as a B-form DNA.[62] It has been previously reported that poly(dG-dC)·poly(dG-dC) undergoes a B-form to Z-form transition under different salt conditions.[63,64] This Z-form conformation of poly(dG-dC)·poly(dG-dC) is stable only under high-salt conditions (4 M NaCl).[62] However, bromination at C8 of the guanine can stabilize the Z-form under low-salt conditions (150 mM NaCl).[65] As shown in panels a and b of Figure 10, titration of neomycin into this duplex does not result in the conformational change until saturation is reached (r_{bd} = 6). A conformational change was observed with the gradual disappearance of the negative band at 247 nm, formation of a new negative band at 295 nm, and the blue shift for the positive band at 270 nm (Figure 10c). All of those features indicate the unexpected formation of a new structure, Z-form DNA. A comparison of a high-salt-induced Z-form with the neomycin-induced structure reveals little difference between the two spectra with one exception, a new positive band at 205 nm (Figure 10d). The opposite patterns observed in the CD spectra appear to be a consequence of the different handedness of the respective polymeric backbones. This result suggests that neomycin induces a left-handed conformation similar in structure to the polyamine-induced Z-form transition observed with methylated $poly(dG\text{-}dC)_2$.[66]

dx.doi.org/10.1021/bi201077h | *Biochemistry* 2011, 50, 9088–9113

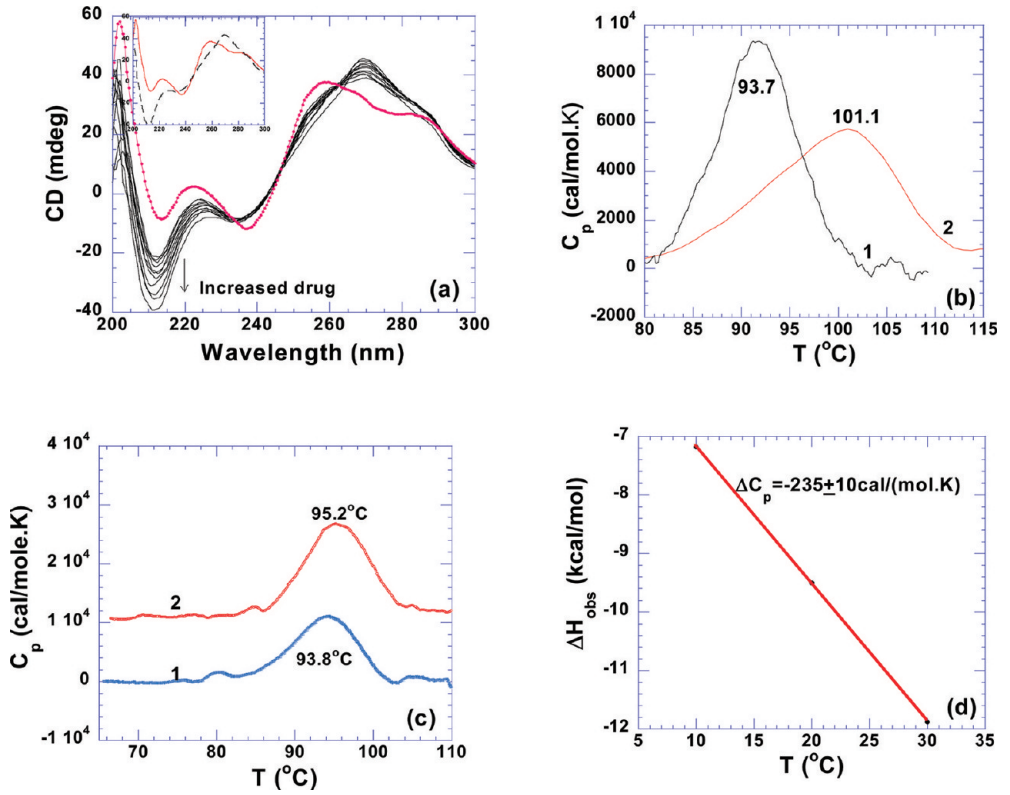

Figure 9. (a) CD scans of neomycin titration with $d(A_2G_{15}C_{15}T_2)_2$ at pH 5.5 (5 μM/duplex). The filled circles show data of DNA by itself. The inset shows the CD spectra of DNA alone (—) and the ligand-saturated complex (---). (b) DSC melting profiles of $d(A_2G_{15}C_{15}T_2)_2$ in the absence (1) and presence (2) of neomycin at an r_{bd} of 10 and pH 5.5 (5 μM/duplex). (c) DSC melting profile of $d(A_2G_{15}C_{15}T_2)_2$ in the absence (1) and presence (2) of neomycin at an r_{bd} of 10 and pH 6.8 (5 μM/duplex). (d) Observed binding enthalpy change for binding of neomycin to $d(A_2G_{15}C_{15}T_2)_2$ at various temperatures and pH 6.8. The experiments were conducted in 10 mM sodium cacodylate, 0.5 mM EDTA, and 100 mM NaCl.

The thermodynamics of poly(dG-dC)·poly(dG-dC) reveals little thermal stabilization caused by neomycin binding (ΔT_m = 1.0 °C) and a small heat capacity change (−28 ± 22 cal mol^{-1} K^{-1}) (Table 3 and Figures S16 and S17 of the Supporting Information).

Calf Thymus DNA. Calf thymus DNA has been found to undergo a transition from B- to Z-form by polyamines such as spermine, spermidine, and putrescine.[67] A recent study has shown that the conformation of calf thymus DNA can be partially converted from B- to A-form by the intercalation of ethidium bromide, acridine orange, and methylene blue.[68] Calf thymus DNA, which contains 42% GC base pairs, was studied with the aim of investigating the GC content dependence of the binding affinity of neomycin with GC-rich sequences. CD spectra of calf thymus DNA show a positive band at 270 nm, a negative band at 247 nm, and a weak band at 210 nm, characteristic of a standard B-form DNA (Figure S18 of the Supporting Information). Titration of neomycin into a DNA solution results in a red shift of the band at 270 nm, indicating base stacking may change toward A-form structure. However, the overall structure of neomycin-bound calf thymus DNA still exhibits the characteristics of the B-form.

Hybrid Duplexes Poly(dA)·Poly(rU) and Poly(rA)·(dT). The DNA·RNA hybrid duplex is believed to adopt an intermediate conformation between the A-form of RNA and the B-form of DNA. Its global structure tends to be closer to the A-form, with the RNA strand containing A-form features and the DNA strand adopting a B-form structure. It has been reported that the hybrid duplex containing a DNA purine strand and an RNA pyrimidine strand (dR·rY) is much less stable than its corresponding reciprocal structure (rR·dY).[69,70] As shown in Figure 11a, poly(dA)·poly(rU) denatures at 43.6 °C, while poly(rA)·poly(dT) melts at 64.7 °C. Previous studies of oligonucleotide hybrid duplexes have shown that DNA·RNA hydrid duplexes exhibit more characteristics of an A-form conformation than a B-form,[71] with the exception of polynucleotide hybrid poly(rA)·poly(dT) that can adopt the B-form conformation under highly solvated conditions.[44]

pH 5.5. As observed in Figure 11b, the CD spectrum of poly(dA)·poly(rU) exhibits a strong positive band at 260 nm and a strong negative band at 210 nm, indicating an A-form conformation. In contrast, a strong negative band at 247 nm and a broad positive shoulder from 270 to 285 nm were observed for poly(rA)·poly(dT), indicating a B-form conformation. A greater heat capacity change was observed for poly(dA)·poly(rU) (−160 ± 18 cal mol^{-1} K^{-1}) than for poly(rA)·poly(dT) (−50 ± 20 cal mol^{-1} K^{-1}) (Table 4 and Figures S19 and S20 of the Supporting Information). A positive binding enthalpy (2.8 kcal/mol) was observed for neomycin binding to poly(dA)·poly(rU) (Figure S20 of the Supporting Information). At low pH, the binding becomes entropically favorable. Factors that contribute to favorable entropy include desolvation of interacting species, a conformational change upon binding, dehydration, and hydrophobic effects.[72] Therefore, the endothermic binding interaction observed between neomycin and poly(dA)·poly(rU) can be explained by one or more of the factors mentioned above. The binding constant for neomycin−poly(dA)·poly(rU) interaction (K_a) was calculated

dx.doi.org/10.1021/bi201077h | *Biochemistry* 2011, 50, 9088–9113

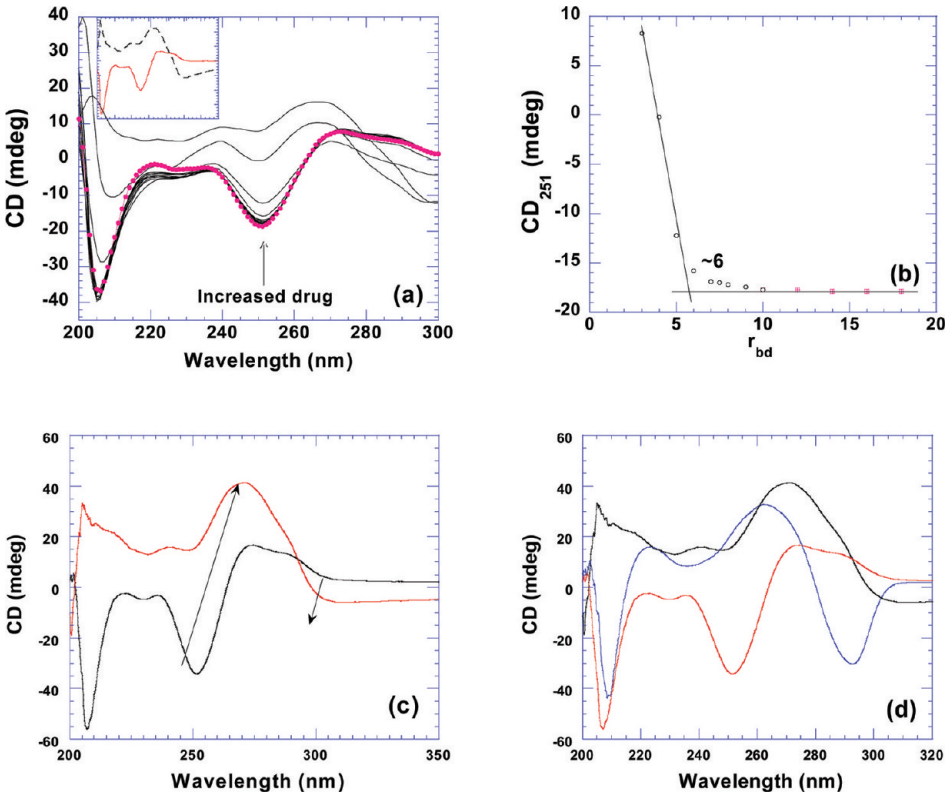

Figure 10. (a) CD titration of neomycin into poly(dG-dC)·poly(dG-dC). The filled circles show the CD spectrum of the DNA by itself. The inset shows the CD spectra of DNA alone (—) and the ligand-saturated complex (---). (b) Plot of CD intensity at 251 nm vs respective r_{bd} values. (c) CD spectra of poly(dG-dC)·poly(dG-dC) B- and Z-form structures. The black line represents that of B-form DNA and the red line that of the neomycin-induced Z-form DNA. (d) Comparison of the CD signals for B-form poly(dG-dC)·poly(dG-dC) (red), the neomycin-induced Z-form poly(dG-dC)·poly(dG-dC) duplex (black), and the high-salt-induced poly(dG-dC)·poly(dG-dC) Z-form structure (blue).[62] The experiments were conducted with 75 μM/bp of DNA in 10 mM sodium cacodylate, 0.5 mM EDTA, and 100 mM NaCl (pH 6.8), with the exception of the high-salt-induced transition that was conducted at 20% (w/w) NaCl.

to be $(9.4 \pm 0.1) \times 10^6$ M^{-1}, approximately 3 times higher than that of poly(rA)·poly(dT) [$(3.4 \pm 0.4) \times 10^6$ M^{-1} (Table 4)].

pH 6.8. At pH 6.8, both poly(rA)·poly(dT) and poly(dA)·poly(rU) adopt conformations similar to those observed at pH 5.5 (Figure S21 of the Supporting Information), indicating that the pH has no effect on hybrid structures. Neomycin stabilizes poly(dA)·poly(rU) significantly at both low and high pH, increasing the melting temperature to ~20 °C at saturated drug ratios (Figures S20–S24 of the Supporting Information). This thermal stabilization induced by neomycin is much greater than that of the well-known intercalator for DNA·RNA hybrids, ethidium bromide.[30]

RNA Duplex 16S A-Site rRNA. The natural target of aminoglycosides, 16S A-site rRNA, has been studied extensively over the past two decades. The binding of the aminoglycosides has been shown to disrupt codon–anticodon interaction on the rRNA leading to erroneous protein synthesis.[1] It has been previously shown that neomycin-class aminoglycosides target a specific conserved sequence in the 16S rRNA A-site of the 30S ribosomal subunit.[73] The first molecular insights into aminoglycoside–A-site binding were obtained for paromomycin and gentamicin C1a using NMR.[2,74] Later, X-ray crystal structures were reported for paromomycin,[75] tobramycin,[76] and Geneticin[77] bound to RNA sequences containing the A-site. We have conducted ITC titrations of neomycin with the 16S A-site rRNA at a pH at which all amino protons on neomycin are protonated, and under solution conditions identical to those used for other nucleic acids in this work.

pH 5.5. Figure 12a shows the CD spectra showing the titration of 16S A-site rRNA by neomycin. The titration of neomycin gradually increases the intensity at 210 and 265 nm, with no changes at other wavelengths. The induced CD signal at 265 or 210 nm can be plotted with the respective r_{bd} ratios, yielding the binding site size of one ligand per RNA molecule (Figure 12b). However, it has been shown that binding of neomycin to 16S A-site rRNA exhibits two binding events with ligand:duplex binding stoichiometries of ~1:1 and ~2:1 using ITC.[7] This second binding event was not detected using CD. The enthalpy of binding of neomycin to 16S A-site rRNA was found to be −2.4 kcal/mol at 20 °C, contributing a 23% driving force to the binding free energy (Table 4, Figure 23, and Figure S25 of the Supporting Information). The association constant of neomycin binding was found to be $(8.7 \pm 0.9) \times 10^7$ M^{-1}, the highest among those of all the nucleic acids studied in this work (Table 4). The thermal stability increase upon neomycin binding was found to be ~7 °C (Figure 12c).

pH 6.8. Titration of neomycin into the 16S A-site rRNA at pH 6.8 yielded a binding event similar to that found at pH 5.5. The thermal stability increase induced by neomycin was found to be smaller at pH 6.8 than at pH 5.5 [$\Delta T_m \sim 4$ °C (Figure S26 of the Supporting Information)], indicating better stabilization of the RNA in the drug-protonated state. Furthermore, the heat capacity change derived from ITC titration (-350 ± 20 cal mol^{-1} K^{-1}) is more than 2 times higher than that obtained at pH 5.5 (-151 ± 12 cal mol^{-1} K^{-1}) (Tables 3 and 4 and Figures S25 and S27 of the Supporting

dx.doi.org/10.1021/bi201077h | Biochemistry 2011, 50, 9088–9113

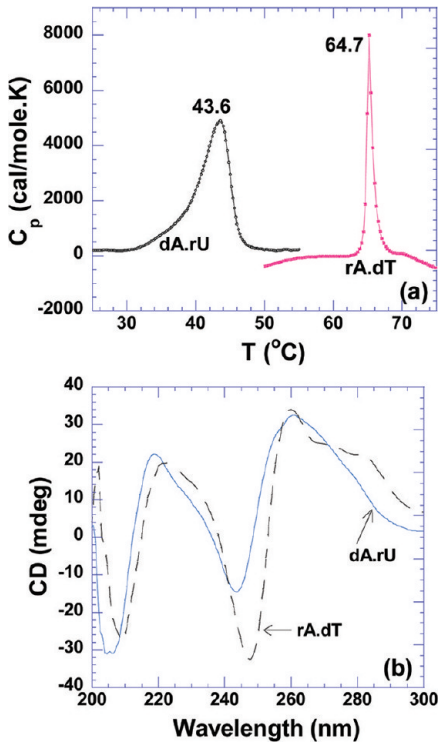

Figure 11. (a) DSC melting profiles of dA·rU and rA·dT (150 μM/bp). (b) CD scans of rA·dT and dA·rU hybrids at 20 °C (40 μM/bp). The experiments were conducted in 10 mM sodium cacodylate, 0.5 mM EDTA, and 100 mM NaCl (pH 5.5).

Information). Such a large discrepancy in the heat capacities can be attributed to the large binding-induced ligand protonation heats at higher pH values.[7]

RNA Duplex Poly(rA)·Poly(rU). Poly(rA)·poly(rU) was first reported in solution by Warner.[78] The conformation of poly(rA)·poly(rU) is an A-form conformation. An equimolar mixture of poly(rA) and poly(rU) does not necessarily form a duplex. The poly(rA)·2poly(rU) triplex can be induced at higher temperatures,[79] high salt concentrations, or low pH values or in the presence of magnesium ions.[51] The nature of species present at a 1:1 poly(rA):poly(rU) ratio triggered much debate in the 1960s and 1970s. Warner concluded that duplex species were present.[80] Fresco, on the other hand, concluded that a three-stranded poly(rA)·2poly(rU) complex formed at equilibrium regardless of the relative proportion of poly(rA) and poly(rU) in the mixture.[81] Miles and Frazier demonstrated directly the existence of duplex poly(rA)·poly(rU) using infrared spectroscopy under various ionic conditions.[82] This result was confirmed by Stevens and Felsenfeld.[79] It has been suggested that the hypochroism observed at 280 nm as the temperature increases corresponds to the denaturation of duplex poly(rA)·poly(rU) and the rearrangement of poly(rA) and poly(rU) to form the three-stranded poly(rA)·2poly(rU) species and free poly(rA).[79] Upon being heated further, the three-strand complex then denatures to a single-stranded coil form. The formation of poly(rA)·2poly(rU) in an equimolar mixture of poly(rA) and poly(rU) has been demonstrated by Blake and Fresco[83] to be the transient byproduct in the formation of poly(rA)·poly(rU), which disappears very slowly (~72 h) in 200 mM Na^+. Thus, the discrepancies observed by different groups could be attributed to the kinetics of duplex formation.

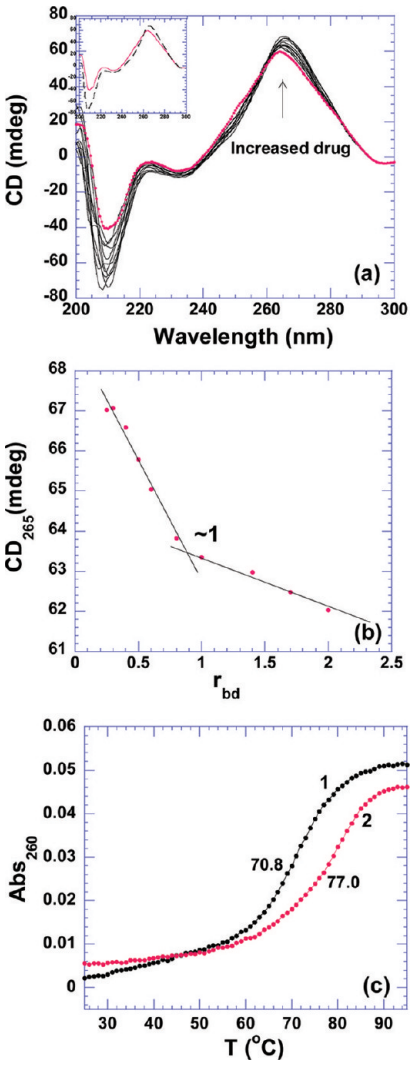

Figure 12. (a) CD scans of the titration of neomycin with 16S A-site rRNA. The filled circles show data of RNA by itself. The inset shows the CD spectra of RNA alone (—) and the ligand-saturated complex (---). (b) Plot of the change in CD signals at 265 nm vs corresponding r_{bd} values. The intersection of two apparent linear sections reveals the binding site size. (c) UV thermal denaturation profiles of RNA in the absence (1) and presence (2) of neomycin at an r_{bd} of 1. The experiments were conducted with 10 μM rRNA in 10 mM sodium cacodylate, 0.5 mM EDTA, and 100 mM NaCl (pH 5.5).

pH 5.5. As shown in Figure 13a, in the presence of neomycin, poly(rA)·poly(rU) disproportionates into the poly(rA)·2poly(rU) triplex and single-stranded poly(rA), which is observed in the large decrease in absorbance at 280 nm. The triplex then denatures directly from 3 to 1 at 81.6 °C. The midpoint of the denaturation of poly(rA)·poly(rU) was used as the melting temperature of this duplex in the presence of the ligand. In the absence of neomycin, disproportionation of poly(rA)·poly(rU) was not observed under the conditions used here (Figure 13a).

Poly(rA)·poly(rU) adopts a canonical A-form conformation, observed as a strong positive band at 260 nm and a negative band at 210 nm in CD spectra (Figure 13b). Binding of neomycin favors the RNA conformation moving toward more A-form conformation, indicated by the increased intensity at these two peaks. Binding of neomycin with this RNA duplex is entropy-driven, even exhibiting an endothermic heat of

dx.doi.org/10.1021/bi201077h | *Biochemistry* 2011, 50, 9088–9113

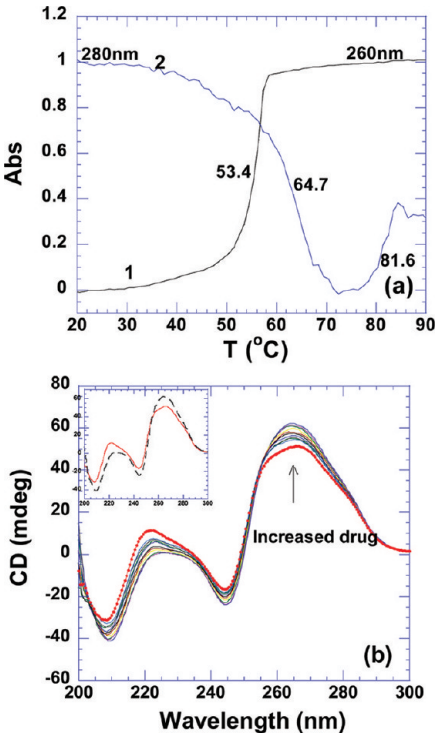

Figure 13. (a) UV melting profiles of poly(rA)·poly(rU) in the absence (1) and presence (2) of neomycin at an r_{bd} of 8. (b) CD titration of poly(rA)·poly(rU) (75 μM/bp) with neomycin. The filled circles show the data for RNA alone. The inset shows the CD spectra of RNA alone (—) and the ligand-saturated complex (---). The experiments were conducted in 10 mM sodium cacodylate, 0.5 mM EDTA, and 100 mM NaCl (pH 5.5).

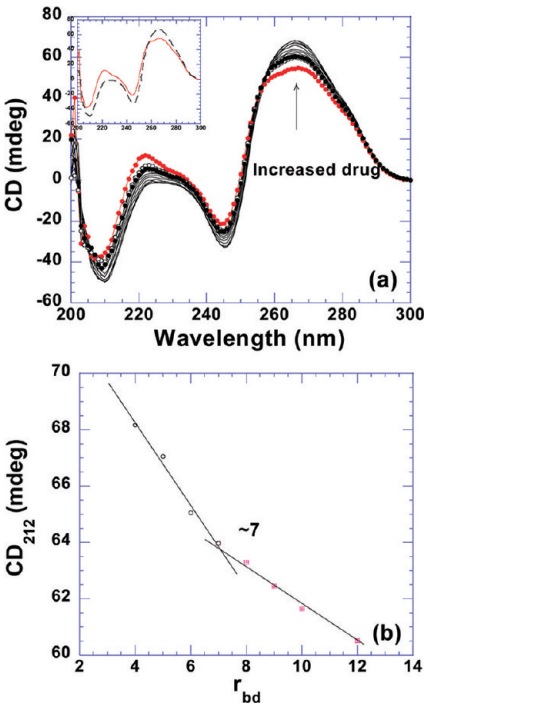

Figure 14. (a) CD titration of poly(rA)·poly(rU) (75 μM/bp) with neomycin. The filled circles show data for RNA alone. The inset shows the CD spectra of RNA alone (—) and the ligand-saturated complex (---). (b) Plot of CD signals at 243 nm vs corresponding r_{bd} values for binding site size determination. The experiments were conducted in 10 mM sodium cacodylate, 0.5 mM EDTA, and 100 mM NaCl (pH 6.8).

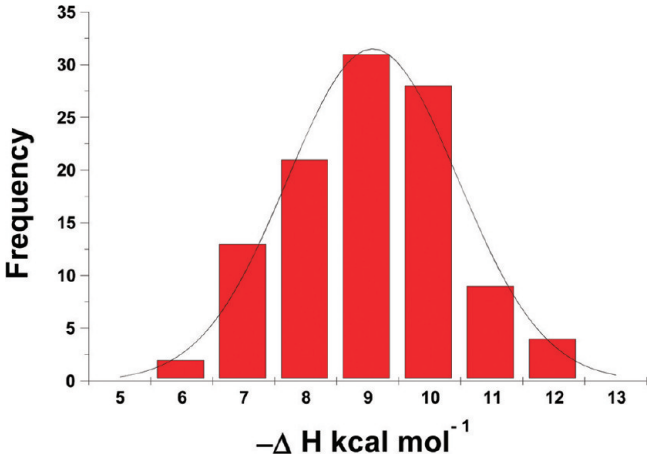

Figure 15. Gaussian distribution of enthalpy values in four separate ITC excess site titration experiments with neomycin and poly(rA)·poly(rU) (150 μM/bp). The experiments were conducted in 10 mM sodium cacodylate, 0.5 mM EDTA, and 100 mM NaCl (pH 6.8) at 30 °C.

interaction at low temperatures (Table 4 and Figure S28 of the Supporting Information). The temperature increase led to diminished contribution from entropy, but it still remained the dominating factor (Table 4 and Figure 23). Poly(rA)·poly(rU) exhibited a high binding constant with neomycin [K_a = (2.9 ± 0.1) × 10^7 M^{-1} (Table 4)].

pH 6.8. It has been reported that magnesium can induce the poly(rA)·2poly(rU) triplex in equimolar solutions of poly(rA) and poly(rU).[51] Neomycin, a polycation with at least five positive charges, induces the formation of triplex RNA at low pH. However, continuous variation and CD spectroscopy showed that titration of neomycin into the poly(rA)·poly(rU) duplex at high pH does not convert the spectrum toward that of a neomycin–poly(rA)·2poly(rU) complex (Figure 14a) under the experimental conditions used here. CD titration with neomycin revealed a binding site size of 7 bp/duplex. (Figure 14b). ITC titrations utilizing the "model-free"[84] method that improves the accuracy of ΔH determination by plotting a large population of individual heat bursts versus their relative frequencies were conducted to assess the accuracy of single excess site ΔH values. Four separate experiments were performed in which 30 ΔH values from 10 μL injections at a low ligand concentration (2 μM) and excess nucleic acid (150 μM/bp) were recorded (Figure S29 of the Supporting Information). The titrations were then plotted as a function of ΔH versus relative frequency. A Gaussian curve fit of the data yielded a ΔH of −9.1 ± 0.3 kcal/mol at 30 °C (Figure 15). A single excess site titration ΔH yielded an enthalpy of binding of −9.8 ± 0.1 kcal/mol (Table 3 and Figure S30 of the Supporting Information), which constitutes a <10% error for single excess site titrations.

Triplex Poly(dA)·2Poly(dT). Triplex DNA or RNA can be formed by associating the triplex-forming single strand with a duplex via Hoogsteen hydrogen bonds in the major groove. The solution conformation of DNA triplex poly(dA)·2poly(dT) has been debated. Evidence of a C3′-endo sugar pucker that is characteristic of the A-form conformation[85] and a C2′-endo sugar pucker that is indicative of a B-form conformation[86] has been reported. It is likely that the poly(dA)·2poly(dT)

dx.doi.org/10.1021/bi201077h | *Biochemistry* 2011, 50, 9088–9113

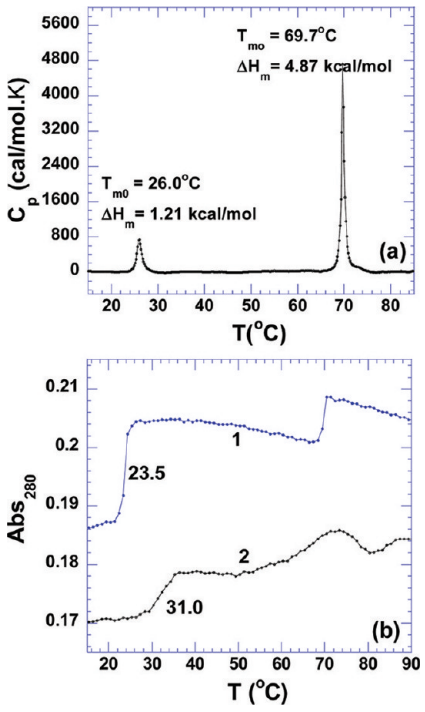

Figure 16. (a) DSC melting profile of poly(dA)·2poly(dT) (100 μM/base triplet). (b) UV melting profiles of triplex in the absence (1) and presence (2) of neomycin at an r_{bd} of 6. The experiments were conducted in 10 mM sodium cacodylate, 0.5 mM EDTA, and 100 mM NaCl (pH 5.5).

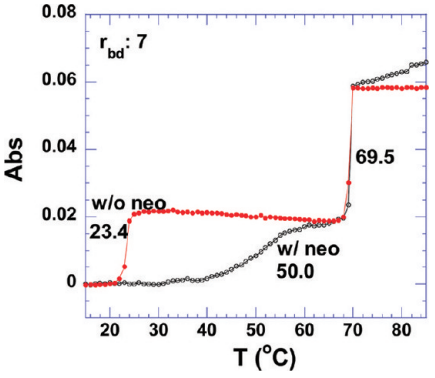

Figure 17. UV thermal denaturation profiles of poly(dA)·2poly(dT) in the absence (1) and presence (2) of neomycin at an r_{bd} of 7. The experiments were conducted in 10 mM sodium cacodylate, 0.5 mM EDTA, and 100 mM NaCl (pH 6.8).

structure contains conformational features that are intermediate between those of A- and B-form conformations.

Aminoglycosides have a significant stabilizing effect on triplex thermal stability. Of all aminoglycosides studied, neomycin was discovered to have the highest level of thermal stabilization on triplex DNA.[25]

pH 5.5. As shown in Figure 16a, the DSC melting profile confirms the formation of the poly(dA)·2poly(dT) triplex, with the enthalpy of triplex melting (1.26 kcal/mol) being ~4 times smaller than that of the corresponding duplex melting (4.87 kcal/mol). The melting temperature of the poly(dA)·2poly(dT) triplex shows a slight concentration dependence, with the one observed in the DSC profile (26.0 °C, 100 μM/base triplet) being 2.5 °C higher than that obtained from the UV

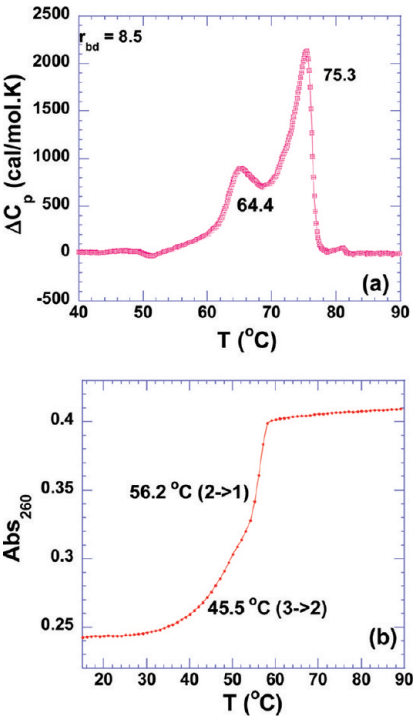

Figure 18. (a) DSC melting profile of poly(rA)·2poly(rU) (100 μM/base triplet) in the presence of neomycin at an r_{bd} of 8.5 and pH 6.8. (b) UV melting profile of poly(rA)·2poly(rU) alone at pH 5.5. The experiments were conducted in 10 mM sodium cacodylate, 0.5 mM EDTA, and 100 mM NaCl.

melting profile (23.5 °C, 15 μM/base triplet) (Figure 16b). The addition of neomycin (r_{bd} = 6) to the DNA triplex does not affect duplex stability. However, it stabilized the triplex thermal stability by 7.5 °C as shown in Figure 16b. These results suggest that neomycin selectively stabilizes the triplex under physiological conditions. ITC excess site titrations at various temperatures yield a large heat capacity change, -264 ± 30 cal mol^{-1} K^{-1} (Table 4). The binding constant of neomycin interacting with the DNA triplex at pH 5.5 (K_a) was found to be $(2.4 \pm 0.1) \times 10^5$ M^{-1} (Table 4 and Figure S31 of the Supporting Information).

pH 6.8. As expected, the binding enthalpy of neomycin interacting with poly(dA)·2poly(dT) is larger at pH 6.8 than at pH 5.5 (Tables 3 and 4 and Figures S31 and S32 of the Supporting Information). Neomycin shows enhanced thermal stability with the DNA triplex at pH 6.8 and an r_{bd} of 7 (Figure 17 and Figure S33 of the Supporting Information). However, at pH 5.5, the neutralization of the DNA triplex (three negatively charged polymers) potential leads to a weakened interaction with the positively charged ligand, as evidenced by a smaller increase in the triplex denaturation temperature (Figure 16b).

Triplex Poly(rA)·2Poly(rU). Recognition of the RNA triplex has not attracted much attention even though it was the first three-stranded nucleic acid reported.[87] The RNA triplex adopts a C_3'-endo sugar pucker characteristic of the A-form conformation. Ligands like sanguinarine, berberine,[88] and berenil[89] have been shown to bind to the RNA triplex. Neomycin stabilizes the RNA triplex more significantly than the DNA triplex.[21] The DSC melting profile reveals that RNA triplex poly(rA)·2poly(rU) exhibits the same thermal stability as its corresponding duplex at pH 6.8 [T_m ~ 59 °C (Figure S34 of the Supporting Information)]. The denaturation of the

dx.doi.org/10.1021/bi201077h | *Biochemistry* 2011, 50, 9088–9113

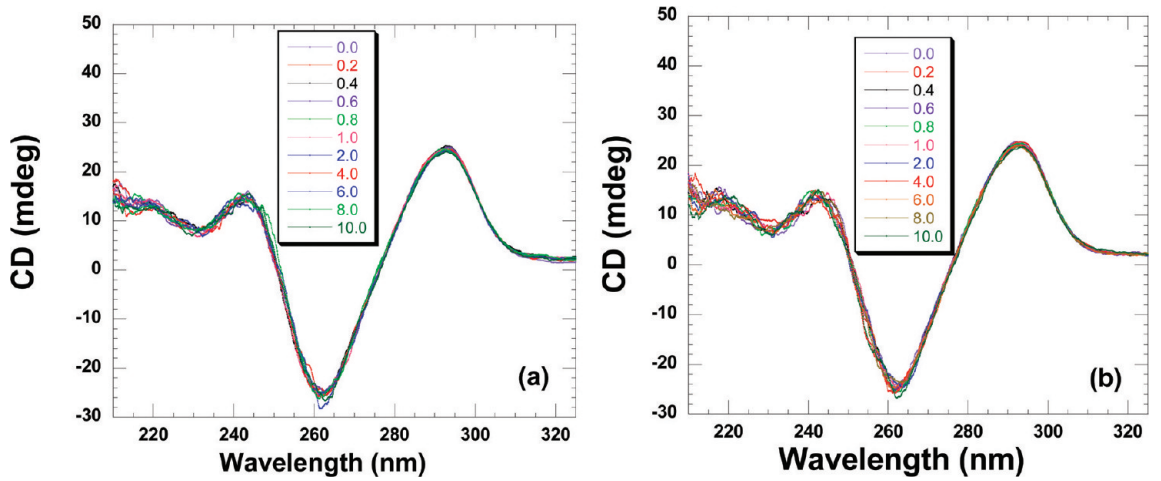

Figure 19. CD titration of the *O. nova* quadruplex (10 μM/strand) with neomycin. A concentrated solution of neomycin was added to the DNA solution followed by a 5 min equilibration. The DNA:ligand ratios are depicted on each graph. The CD scans are averages of two scans. The titrations were conducted in 10 mM sodium cacodylate, 0.5 mM EDTA, and 100 mM NaCl at (a) pH 5.5 and (b) 6.8.

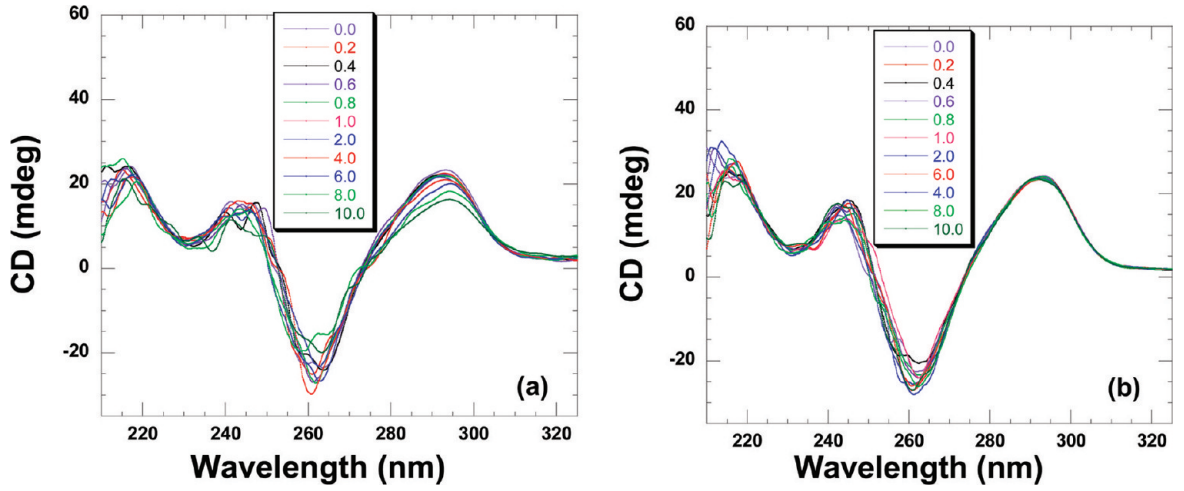

Figure 20. CD titration of the human telomeric quadruplex (10 μM/strand) with neomycin. A concentrated solution of neomycin was added to the DNA solution followed by a 5 min equilibration. The DNA:ligand ratios are depicted on each graph. The CD scans are averages of two scans. The titrations were conducted in 10 mM sodium cacodylate, 0.5 mM EDTA, and 100 mM NaCl at (a) pH 5.5 and (b) 6.8.

triplex dissociates the three strands directly to the single strand with a melting enthalpy of 5.5 kcal/mol. This enthalpy of melting of three strands, as expected, is much larger than the enthalpy of melting of the DNA triplex to the duplex and a single strand (1.0 kcal/mol). However, it is comparable to the melting enthalpy obtained from the corresponding RNA duplex denaturation (6.8 kcal/mol).[90] The RNA triplex forms easily even in the equimolar ratio mixture of poly(rA) and poly(rU).[81] In the presence of neomycin, two melting transitions in the DSC melting profile are observed for poly(rA)·2poly(rU) at pH 6.8 (Figure 18a and Figure S34 of the Supporting Information). Similarly, at pH 5.5, two melting transitions were observed in the UV experiment: one at 45.5 °C identified as the triplex melting to single strands and the other at 56.2 °C identified as the duplex melting to single strands (Figure 18b). However, these two melting transitions are too close in the DSC melting profile for an accurate determination of melting enthalpies for each transition. This ambiguity prevents an accurate calculation for the melting enthalpy of the RNA triplex and precludes the determination of a binding constant using the ΔT_m method (Figure S35 of the Supporting Information).

Quadruplexes. Four guanine-rich DNA strands can associate to form a quadruplex structure under physiological conditions. The formation of a G-quadruplex involves eight hydrogen bonds formed through Hoogsteen pairing where four guanines orient themselves in either a parallel or an antiparallel orientation. The G-rich quadruplex structure can adopt a diverse pattern of folding, resulting from variations in loop size and sequence and the possible combinations of strand orientation. The binding of small molecules to the quadruplex structure has been intensely researched in recent years.[91]

To date, most molecules found to bind to the quadruplex are intercalators with a planar structural feature. Most of these planar aromatic moieties bind to their host quadruplex DNAs with moderate affinities ($K_a \sim 10^5$ M^{-1}). Their binding affinities are also highly dependent on the structure of quadruplex DNA.[92,93] While most of the G-quadruplex binding molecules discovered so far have been shown to have non-groove binding interactions, only a handful of molecules have been characterized to have interactions in the groove.[94] We

dx.doi.org/10.1021/bi201077h | *Biochemistry* 2011, 50, 9088–9113

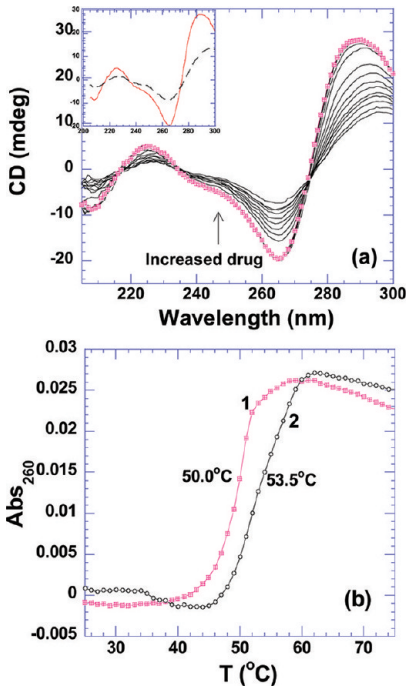

Figure 21. (a) CD titration of neomycin into i-motif DNA (50 μM/bp). The filled circles show data for DNA only. The inset shows CD spectra of DNA alone (—) and the ligand-saturated complex (---). (b) UV melting profiles of i-motif DNA in the absence (1) and presence (2) of neomycin at an r_{bd} of 4. The experiments were conducted in 10 mM sodium cacodylate, 0.5 mM EDTA, and 100 mM NaCl (pH 6.8).

studied the binding of aminoglycosides to a well-characterized quadruplex formed by the telomeric DNA of *Oxytricha nova* [d(5′-GGGGTTTTGGGG-3′)] and human telomeric DNA [d(5′-AGGGTTAGGGTTAGGGTTAGGG-3′)]. These nucleic acid sequences are known to form an antiparallel quadruplex.[95] In both sodium and potassium ions, the *O. nova* quadruplex is known to have the same overall topology with slight variations in the loop connections.[96] This quadruplex DNA has four grooves that vary in shape and width and have been classified as narrow, wide, and medium (two grooves that are similar in width and are between the groove widths of narrow and wide grooves). Similarly, the unimolecular human telomeric quadruplex also has medium, narrow, and wide grooves.

O. nova Quadruplex. pH 5.5. The formation of the antiparallel quadruplex was checked using CD spectroscopy. As seen in Figure 19a, a positive band at 295 nm and a negative band at 260 nm were observed and are characteristic CD signatures for an antiparallel quadruplex structure.[97] To investigate any binding-induced changes, CD titration experiments were conducted. The DNA solution was serially titrated with a concentrated ligand solution. However, even after additions of large amounts of the ligand, very small changes in the CD signal at 295 or 260 nm were observed (Figure 19). These results indicate that neomycin binding does not perturb the quadruplex structure significantly. UV thermal denaturation experiments showed that the quadruplex melted at 55.9 °C in the absence of ligand (Figure S36 of the Supporting Information). At a 1:1 ligand:quadruplex ratio, the DNA melted at 56.3 °C. ITC experiments showed the heat of ligand−quadruplex interaction to be very small at this pH, <1.0 kcal/mol (Figure S37 of the Supporting Information).

pH 6.8. Similar to observations at pH 5.5, the CD spectrum showed the formation of the quadruplex (Figure 19b). The CD titration with neomycin did not show any significant binding-induced changes. Likewise, there was also a small thermal stabilization upon ligand binding at a 1:1 ligand:quadruplex ratio (Figure S36 of the Supporting Information). The ITC experiments were performed to determine the binding affinities (Figure S37 of the Supporting Information). The ITC-derived binding stoichiometry showed approximately one ligand binding to the quadruplex with an affinity (K_a) of (1.8 ± 0.3) × 10^5 M^{-1} (Table 4).

Human Telomeric DNA. pH 5.5. Human telomeric DNA contains a repeat hexamer unit [d(5′-TTAGGG)]. A 22-mer oligonucleotide model d(5′-AGGGTTAGGGTTAGGGTTAGGG) has been shown to adopt an antiparallel structure in solution.[98] The CD spectrum showed a positive peak at 295 nm and a negative peak at 260 nm that are consistent with the antiparallel structure of the quadruplex (Figure 20a). To characterize the binding-induced structural changes, we conducted CD titration with increasing ligand concentrations. Even after large additions of neomycin to the quadruplex, very small changes in the CD intensity were observed at 295 nm. These results indicate that like *O. nova*, this quadruplex undergoes very small structural changes upon ligand binding, and the overall antiparallel fold of the quadruplex is preserved. The UV thermal denaturation studies showed a small thermal stabilization of <1 °C (Figure S38 of the Supporting Information). Similar to the *O. nova*, because of the low heats of interaction in the ITC studies, the resulting enthalpy profile could not be fitted at this pH (Figure S37 of the Supporting Information).

pH 6.8. As seen from the CD spectrum, the antiparallel structure was confirmed by the positive band at 295 nm. The addition of neomycin resulted in minimal changes in the CD intensity at 295 nm (Figure 20b). Similar to the results at pH 5.5, UV thermal denaturation experiments also showed minimal thermal stabilization (Figure S38 of the Supporting Information). ITC-derived binding constants were obtained using a one-site binding model (Figure S37 of the Supporting Information). The results obtained show that neomycin binds to the human telomeric DNA with a 1:1 ligand:quadruplex ratio with an affinity constant (K_a) of (2.5 ± 0.2) × 10^4 M^{-1} (Table 4).

i-Motif Poly(dC). Cytosine-rich polynucleotides or oligodeoxynucleotides can adopt a non-B-form structure called the i-motif at slightly acidic or neutral pH. This i-motif DNA is a tetramer of equivalent strands, containing two duplexes zipped together in an antiparallel fashion. The individual parallel stranded duplexes have their hemiprotonated C·C^+ base pairs face to face in the right-handed and unwound manner (Figure 1).[99] This structure contains two wide and two narrow grooves.

The cytosine-rich sequence is found at the 5′ end of the telomere in eukaryotic chromosomes[100] and some noncoding regions of eukaryotic DNA such as promoter sites and introns. Some RNA in the genomes of various cardioviruses and encephalomyocarditis viruses contains many stretches composed of more than 75% cytosine.[100]

As shown in Figure 21a, the CD scan of the poly(dC) sequence exhibits a strong positive band at 285 nm and a negative band at 265 nm, both characteristics of the i-motif structure. Titration of neomycin shows the formation of a complex with an isosbestic point at 272 nm. Binding of neomycin at an r_{bd} of 4 increases the thermal stability of the i-

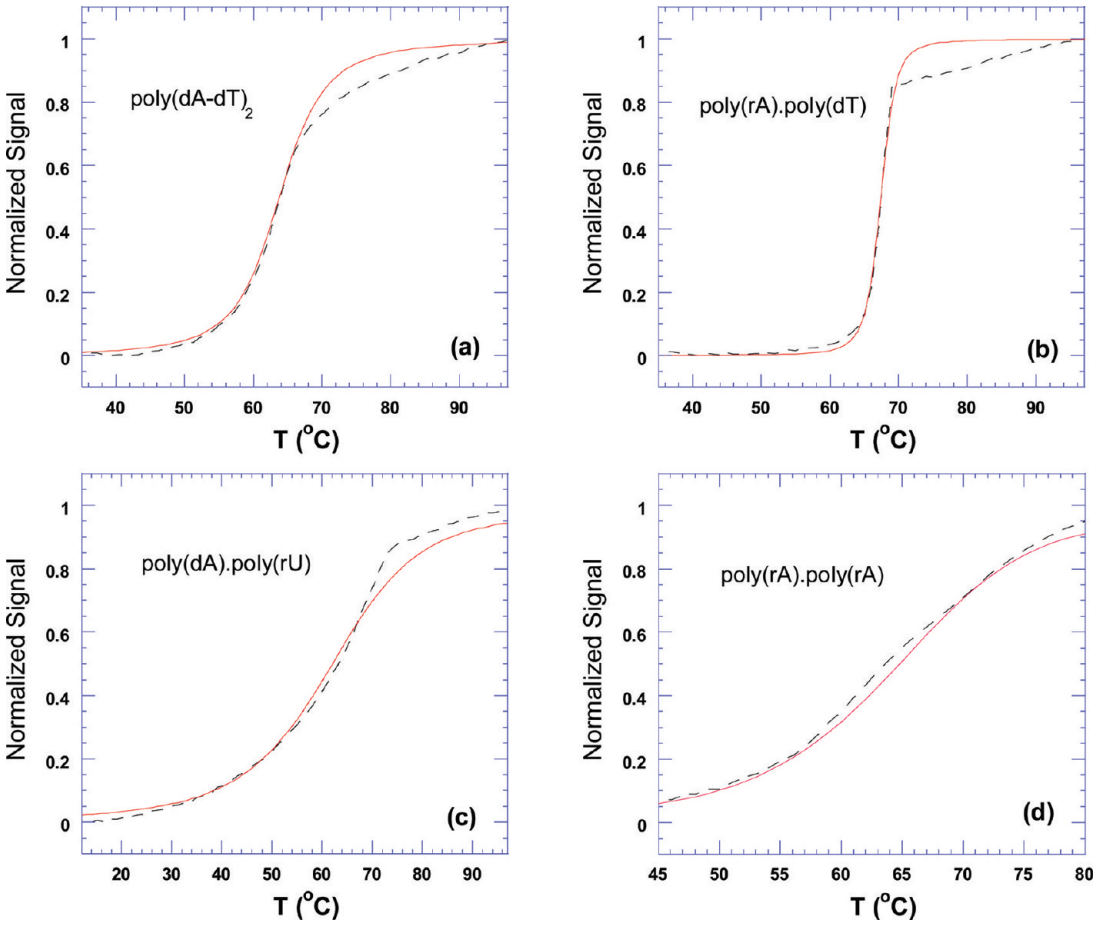

Figure 22. Thermal denaturation plots for DNA duplexes in the presence of neomycin. The dashed black lines represent thermal denaturation curves from experimental data. The red lines represent best fit simulations derived using McGhee's statistical mechanical model.[109] The corresponding simulated McGhee binding affinity values are as follows: (a) 2.0×10^4, (b) 3.4×10^5, (c) 9.4×10^5, and (d) 4.7×10^6 M^{-1}. The experiments were conducted in 10 mM sodium cacodylate, 0.5 mM EDTA, and 100 mM NaCl (pH 5.5).

Table 5. Comparison of Binding Preferences of Neomycin between Competition Dialysis and ΔT_m Method-Derived Binding Constants

	K_a ($\times 10^5$ M^{-1}) via ΔT_m	K_{app} ($\times 10^5$ M^{-1}) via competition dialysis
AT-rich duplexes[a]	0.9 ± 0.1 [poly(dA-dT)$_2$]	0.08 ± 0.02 [poly(dA)·poly(dT)]
poly(dA)·2poly(dT)[a]	11 ± 1 (15 °C)	–
poly(rA)·poly(dT)[a]	34 ± 4	0.17 ± 0.09
poly(dA)·poly(rU)[a]	94 ± 1	0.32 ± 0.04
poly(rA)·poly(rA)[a]	170 ± 20	–
GC-rich duplex[a]	180 ± 60 [d($A_2G_{15}C_{15}T_2$)$_2$]	0.21 ± 0.06 [poly(dG)·poly(dC)]
poly(rA)·2poly(rU)[a]	–	1.00 ± 0.04
poly(rA)·poly(rU)[a]	290 ± 10	0.35 ± 0.07
16S A-site RNA[b]	870 ± 90	17.0 ± 0.5

[a]Obtained via the ΔT_m method. [b]Obtained via ITC data fitting using the one-binding site model.

motif DNA by 4 °C (from 50 to 53.5 °C) as shown in Figure 21b and Figure S39 of the Supporting Information. The binding affinity cannot be accurately calculated using the ΔT_m method because of the contribution of the heat of protonation to enthalpy at pH 6.8.

DISCUSSION

Comparison of Neomycin–Nucleic Acid Interactions at pH 5.5 and 6.8. Aminosugars such as neomycin undergo protonation after forming complexes with DNAs or RNAs.[72] This presents a significant problem in obtaining the intrinsic binding enthalpy and heat capacity change at or near physiological pH. Thus, the binding affinity calculated with the ΔT_m method[7] using these thermodynamic parameters could be overestimated at pH 6.8. Inspection of the pK_a values of the six amino groups on neomycin shows that it is almost fully protonated at pH 5.5.[72] Thereby, enthalpies of binding obtained at this pH reflect values close to the intrinsic heats of binding of neomycin–nucleic acid complexation. Caution, however, must be exercised because a pH of 5.5 can itself induce nucleic acid instability for some structures. In this report, we have reported thermodynamic studies of neomycin

dx.doi.org/10.1021/bi201077h | Biochemistry 2011, 50, 9088–9113

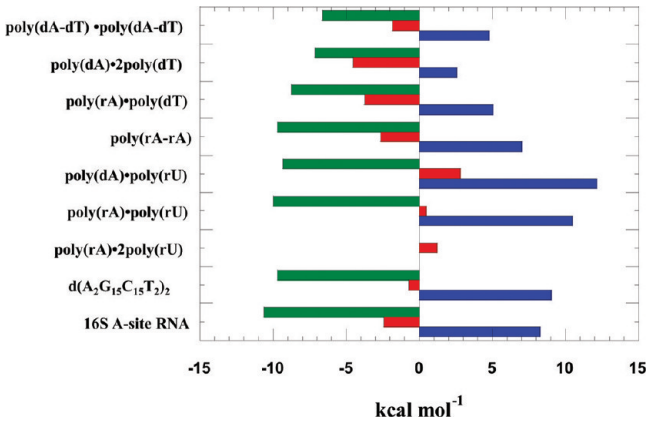

Figure 23. Thermodynamic profile of neomycin–nucleic acid binding. Green bars represent ΔG values, red bars ΔH values, and blue bars $T\Delta S$ values. The experiments were conducted in 10 mM sodium cacodylate, 0.5 mM EDTA, and 100 mM NaCl (pH 5.5).

binding at pH 6.8 and 5.5 to single-strand, duplex, triplex, and quadruplex nucleic acids. The results presented provide a fundamental basis for understanding neomycin's interaction and selectivity for a variety of nucleic acids and can serve as a database for studying binding of aminosugars and modified aminosugars to nucleic acid targets.

The advantage of the study at pH 6.8 is that all the conformations adopted by nucleic acids, their binding site size, melting enthalpy, and thermal stabilization by neomycin reflect binding properties that are indicative of solution conditions much closer to physiological conditions. At pH 5.5, neomycin amines are nearly protonated; thus, the observed binding enthalpy, entropy, and binding constant reflect the intrinsic heat of interaction between the ligand and nucleic acids. However, study at such a low pH can lead to practical problems such as a decreased enthalpy of interaction and alterations in nucleic acid structure and stability. At pH 6.8, the observed binding enthalpy includes the intrinsic binding enthalpy between neomycin and nucleic acid, the binding-linked heat of protonation, and the dilution heat of the ligand. The dilution heat can be obtained experimentally by titrating the ligand solution into buffer only. The protonation heat of neomycin differs from system to system, depending on the extent of binding-linked protonation, and thus contributes differently to the observed ΔC_p and binding constants. The overestimated binding enthalpy obtained from ITC experiments at pH 6.8 can therefore lead to a slightly higher binding constant with the ΔT_m-based method. ΔT_m-based binding constants at this pH are not reported here, but the observed heats of interaction and T_m changes are listed in Table 3.

A negative ΔC_p was observed for neomycin–nucleic acid interactions at pH 5.5 and 6.8 (Tables 3 and 4). The negative ΔC_p is thought to be a distinctive feature of site-specific binding in protein–DNA interactions. The negative sign partially results from the removal of large amounts of nonpolar surface area upon formation of the complex.[101,102] The solvent-accessible surface area change (ΔSASA) has an impact on the value of ΔC_p, as well.[7,103,104] Removal of nonpolar surface area causes the ΔC_p value to be more negative, while removal of polar surface leads to a more positive ΔC_p value. In addition to removal of nonpolar solvent-accessible surface area, changes in vibrational modes of macromolecules and water molecules,[105] as well as the involvement of the conformational equilibrium of

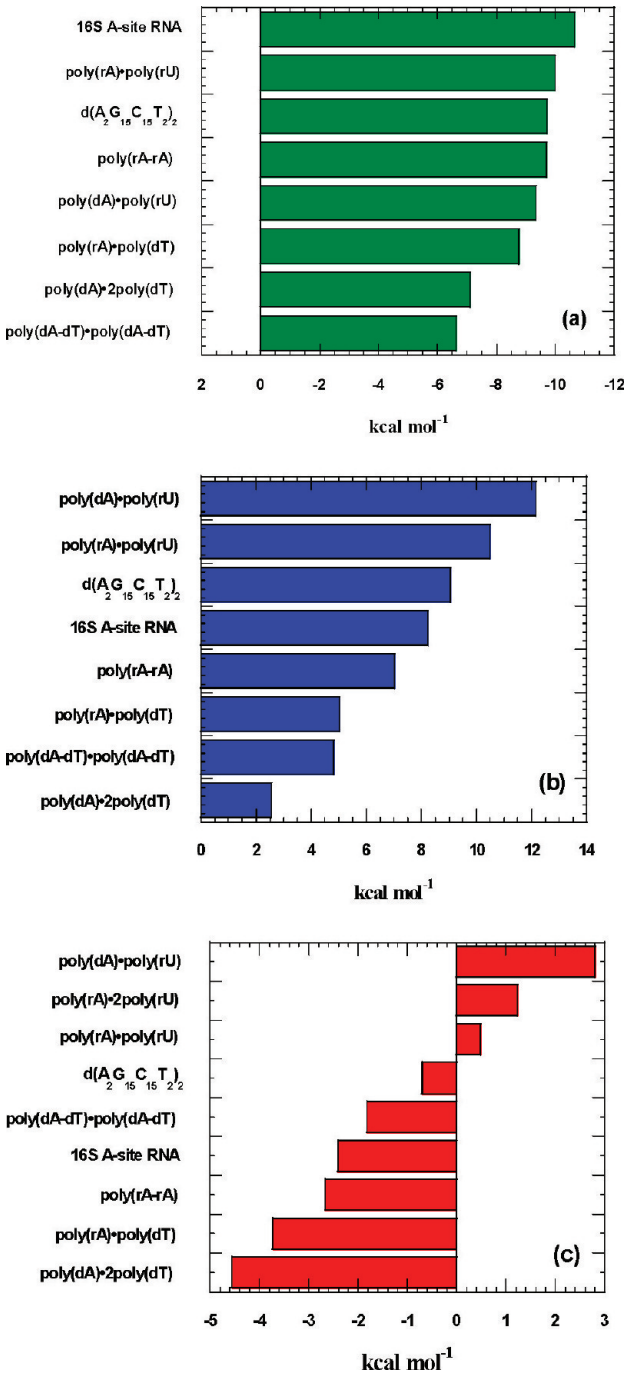

Figure 24. Thermodynamic profile of neomycin–nucleic acid binding separated according to Gibbs free energy equation components (Figure 23) and ranked accordingly: (a) ΔG, (b) $T\Delta S$, and (c) ΔH. The experiments were conducted in 10 mM sodium cacodylate, 0.5 mM EDTA, and 100 mM NaCl (pH 5.5).

macromolecules,[106,107] contribute to the ΔC_p. Binding-coupled protonation of the ligand molecule is also believed to contribute to the observed ΔC_p value at pH 6.8.[108]

Tables 3 and 4 show the thermodynamic parameters obtained for interactions of neomycin with a variety of nucleic acids at pH 6.8 and 5.5, respectively. Several conclusions can be drawn from the results. (1) In the absence of the heat of binding-induced protonation, the binding enthalpies at pH 5.5 are all smaller than the ones observed at pH 6.8. (2) All heat capacity changes at pH 5.5 are smaller than the heat capacity

dx.doi.org/10.1021/bi201077h | Biochemistry 2011, 50, 9088–9113

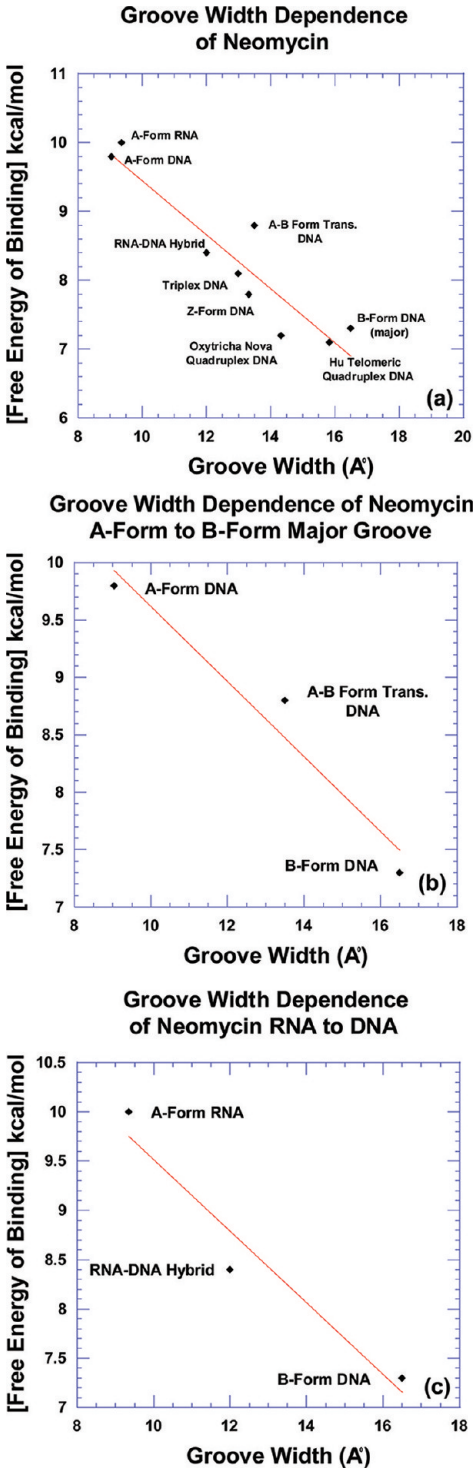

Figure 25. Plot depicting the dependence of the neomycin–nucleic acid complex binding energy (absolute value in kilocalories per mole) on groove width (angstroms): (a) all nucleic acids studied, (b) A-form to B-form structures, and (c) A-form RNA to B-form DNA structures.

changes at pH 6.8, suggesting that at pH 6.8 the temperature dependence of the heats of protonation also contributes to the differences in heat capacity changes of interaction. (3) At pH 6.8 and 5.5, CD titration of neomycin into various nucleic acids as well as FID titrations at pH 6.8 of neomycin into the same (Figures S40–S42 of the Supporting Information) reveals similar binding site sizes. This result indicates that different pH values do not affect the binding sites and modes but may affect the strength of ligand–nucleic acid interaction in addition to the heats of interaction. (4) The order of preference of neomycin for nucleic acid structures observed at pH 5.5 is as follows: A-site RNA > poly(rA)·poly(rU) > GC-rich 34-mer oligonucleotide DNA > poly(rA)·poly(rA) > poly(dA)·poly(rU) > poly(rA)·poly(dT) > poly(dA)·2poly(dT) > poly(dA)·poly(dT).

McGhee's Statistical Mechanical Model-Derived Binding Affinities. Ligand–DNA binding affinities can be determined by using a statistical mechanical model derived from McGhee's theory for the thermal denaturation of ligand-bound DNA.[35] By using T_{mo}, ΔH, n, and ΔH_{wc} from Tables 3 and 4, as well as a nucleation parameter (σ), complete melting curves can be generated. By fitting these models to thermal denaturation data, binding affinities can be computationally simulated.[109] McGhee fits for the thermal denaturation curves of neomycin and nucleic acid duplexes poly(dA-dT)$_2$, poly(rA)·poly(dT), poly(dA)·poly(rU), and poly(rA)·poly(rA) at pH 5.5 are shown in Figure 22. While the McGhee fits produced binding affinities that were consistently lower than the ITC-derived constants (Table 4), the overall trend did not change: poly(rA)·poly(rA) $K_a = 4.7 \times 10^6$ M^{-1}; poly(dA)·poly(rU) $K_a = 9.4 \times 10^5$ M^{-1}; poly(rA)·poly(dT) $K_a = 3.4 \times 10^5$ M^{-1}; poly(dA-dT)$_2$ $K_a = 2.0 \times 10^4$ M^{-1}.

Comparison of Competition Dialysis and ΔT_m Method-Derived Binding Constants of Neomycin Interaction. When comparing the binding preference of neomycin, we calculated the apparent binding constant K_{app} with eq 4[110]

$$K_{app} = C_b/[C_f - ([NA]_{total} - C_b)] \quad (4)$$

where C_b and C_f are the bound and free ligand concentrations, respectively, and $[NA]_{total}$ is the total nucleic acid concentration used in the competition dialysis.

Table 5 shows the binding affinities of neomycin calculated from eq 4 for competition dialysis and the ΔT_m-based method at pH 5.5. DNA triplex poly(dA)·2poly(dT) and poly(rA)·poly(rA) were not used in competition dialysis because these structures do not exist at pH 7.0 under the salt conditions used for this comparison. Poly(rA)·2poly(rU) triplex–neomycin binding affinity also cannot be derived with the ΔT_m method because of the aforementioned reasons.

The order of binding preferences of neomycin observed from competition dialysis is as follows: 16S A-site rRNA > RNA triplex poly(rA)·2poly(rU) > RNA duplex poly(rA)·poly(rU) > poly(dG)·poly(dC) and poly(dA)·poly(rU) > poly(rA)·poly(dT) > poly(dA)·2poly(dT). The trend observed from ΔT_m-derived binding affinities at pH 5.5 follows the same general trend: 16S A-site rRNA > poly(rA)·poly(rU) > d($A_2G_{15}C_{15}T_2$)$_2$ > poly(rA)·poly(rA) > poly(dA)·poly(rU) > poly(rA)·poly(dT) > poly(dA)·2poly(dT) > poly(dA-dT)$_2$.

Remarkably, both methods exhibit approximately the same order of binding preference of neomycin over the range of nucleic acids studied. The binding constants obtained from competition dialysis are all smaller in magnitude than those observed by the ΔT_m-based method. The discrepancy could be due to the fact that unlike the excess site ITC titrations, the affinities derived from competition dialysis are averages of affinities for specific as well as the weaker, nonspecific ligand binding events that occur at higher concentrations for the polycation–nucleic acid interactions studies here. Other factors such as the effect of the dye on neomycin binding and the

dx.doi.org/10.1021/bi201077h | Biochemistry 2011, 50, 9088–9113

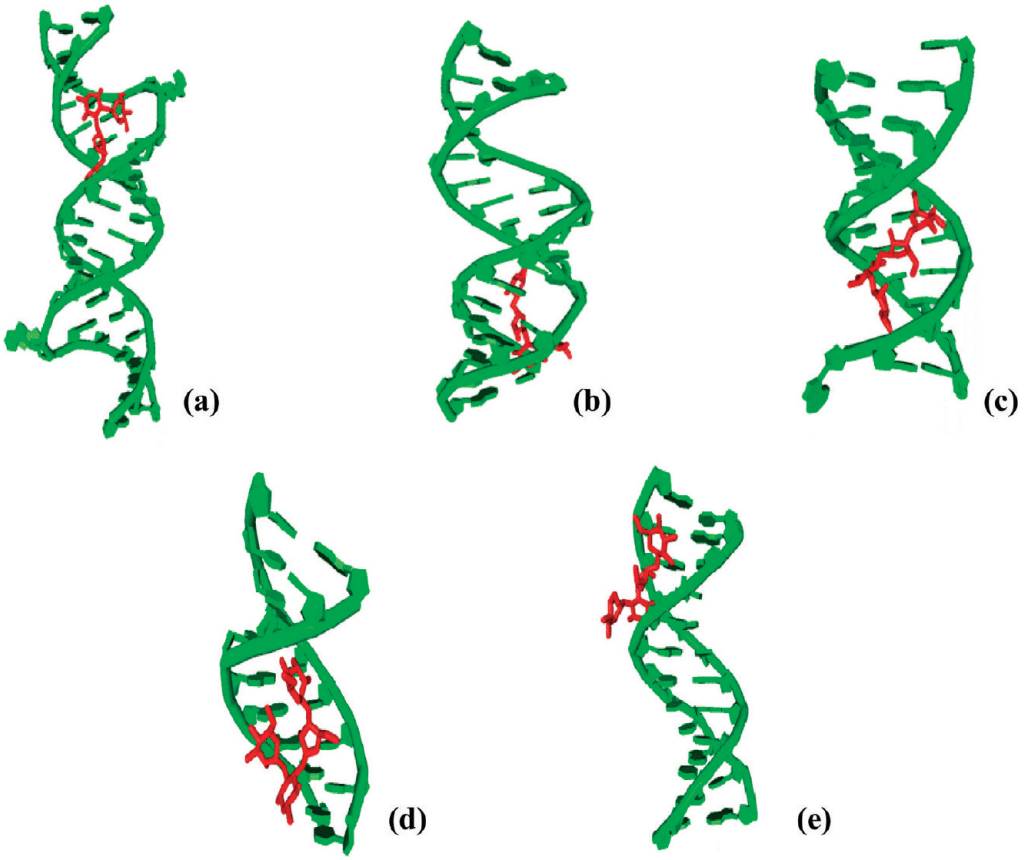

Figure 26. Computer-generated models for neomycin bound to various nucleic acids as suggested by docking studies: (a) A-site RNA, (b) A-form RNA duplex, (c) A-form DNA duplex, (d) RNA·DNA hybrid duplex, and (e) B-form DNA.

binding of F-neo to the dialysis membrane cannot be ruled out. Therefore, as previously suggested,[111] for an accurate determination of binding constants, a rigorous calorimetric treatment is clearly the method of choice. Though competition dialysis may not quantitatively distinguish the binding affinities for primary binding sites, it still can be used qualitatively as an efficient technique to compare the binding preference of neomycin with various nucleic acids, even where weaker secondary binding events may be operable.

The thermodynamic properties for neomycin–nucleic acid interactions are displayed as bar graphs (Figure 23). Individual thermodynamic contributions for neomycin bound to the nucleic acids are mostly entropically driven. As previously stated, all neomycin amines are close to being fully protonated at pH 5.5, which minimizes enthalpic contributions from binding-induced protonation. Accordingly, all structures exhibit large positive entropy values that can be attributed to factors such as desolvation, conformational shifts, and the liberation of counterions as well as water. Interactions with high-affinity A-form structures such as poly(rA)·poly(rU) display the highest positive entropy values. As the structures undergo the transition from the A-form to the B-form, ligand affinities are gradually reduced. High-affinity structures such as the 16S A-site RNA were used as a control and represent a special case of an RNA secondary structure. Neomycin binding to 16S A-site RNA exhibits negative enthalpies. Poly(rA)·2poly(rU) binding data shows an incomplete thermodynamic profile due to the disproportionation of the structure at this pH. A comparison of ΔG values is shown in Figure 24a. As expected, the good potential and shape complements found in A-form structures generate the most negative free energies of binding. Additionally, the higher-affinity A-form DNA–ligand interactions are more entropically driven than lower-affinity B-form DNA–ligand binding (Figure 24b). ΔH values range from low positive heats for A-form RNA and hybrid structures to negative heats for B-form structures (Figure 24c).

Docking Studies. In the analysis of the various DNA and RNA structures studied in this work, the groove width of the nucleic acid structures appears to strongly impact the binding affinity of neomycin. As seen in Figure 25, the binding of neomycin to various forms of DNA and RNA correlates roughly with the width of the nucleic acid groove. Figure 25a displays the general survey trend from A-form RNA to B-form DNA. As the structures undergo the transition from the A-form to the B-form and RNA to AT-rich DNA, the free energy of binding decreases as the groove width increases to produce a shallower and wider pocket. The modeling results also correlate well with the entropic contribution to binding [the smaller the groove width, larger the entropic contribution (Figure 24b)]. This phenomenon is succinctly expressed by Figure 25b. The same trend is further supported by Figure 25c.

Overall, a strong correlation is seen for the affinity of neomycin for the major groove width of nucleic acid structures, and the increase in binding energy correlates well with a decrease in major groove width (A-form RNA > A-form DNA > DNA·RNA hybrid and triplex > B-form DNA and quadruplex DNA) (Figure 26 and Tables S1–S3 of the Supporting Information).

dx.doi.org/10.1021/bi201077h | *Biochemistry* 2011, 50, 9088–9113

CONCLUSION

An attempt has previously been made to depict distinct qualitative differences between the thermodynamic profiles for groove binding and intercalating ligands.[112] Figure 27 is a reproduction of the figure from that study.[112] Two distinct groups emerge from the thermodynamic comparison of ΔH with $-T\Delta S$: groove binders (○) and intercalators (●).[112] The filled squares added to the figure represent the individual thermodynamic profiles from the neomycin−duplex hybrid and higher-order structures studied in our work. Their grouping and placement within the groove binder profile are consistent with neomycin's known major groove binding mode. Figure 28 extrapolates this thermodynamic comparison by applying the plot to all neomycin−nucleic acid structures studied here at pH 5.5. Analysis indicates that a structural trend is evident with the emergence of two distinct groups: A-form (red) groove binders and B-form (blue) groove binders (Figure 28).

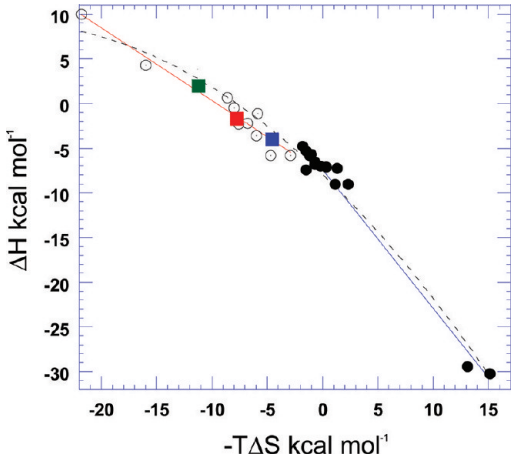

Figure 27. Reproduction of the compensation plot for DNA−ligand binding plotted as a function of ΔH vs $-T\Delta S$ from Chaires.[112] The empty circles represent data for groove binding DNA duplex binders.[112] The filled circles represent data for intercalators.[112] The three colored squares represent data for neomycin−nucleic acid duplex interactions: poly(dA)·poly(rU) (green), poly(rA)·poly(dT) (blue), and $d(A_2G_{15}C_{15}T_2)_2$ (red) at pH 5.5 and 25 °C.

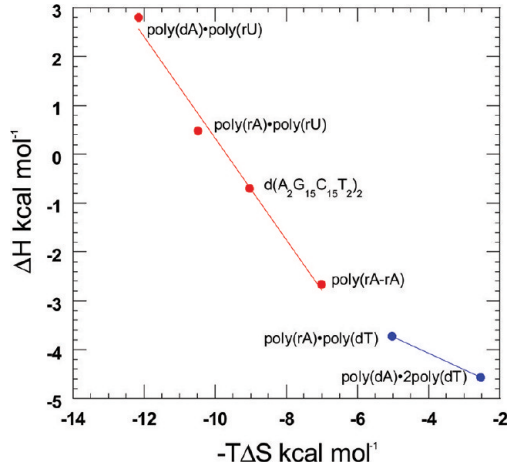

Figure 28. Compensation plot for neomycin−nucleic acid binding interactions plotted as a function of ΔH vs $-T\Delta S$ at pH 5.5 and 25 °C.

Since the discovery of aminoglycosides as RNA binders three decades ago, their nucleic acid targets have grown to include multistrand DNA structures such as triplexes and quadruplexes. This study investigates a variety of nucleic acid structures in our evaluation of neomycin's binding properties and extraction of thermodynamic parameters of binding. Results obtained from this study suggest that neomycin prefers to bind A-form-like nucleic acid structures, gradually becoming less favorable as nucleic acid structures undergo the transition to the B-form. This report, the first involving a nucleic acid screen by neomycin from a thermodynamic perspective, can function as a database for comparing modified aminoglycoside ligands.

A different perspective on the results obtained from this study also comes from our developing understanding of nucleic acid recognition. As it is becoming increasingly evident from studies of protein−DNA recognition, shape readout of DNA in addition to direct readout mechanisms is extremely important.[113−116] Small molecule-based approaches to nucleic acid recognition should therefore include approaches that use nucleic acid shape readout with the ability to detect local variations in DNA shape and electrostatic potential, as shown here, in addition to existing "direct readout" approaches utilized in the development of small molecule DNA minor groove binding ligands.

ASSOCIATED CONTENT

Supporting Information

UV and DSC melting profiles of all nucleic acid structures, CD titration curves of neomycin with all structures, ITC excess-site titration curves at various temperatures, table of all thermodynamic parameters used in calculating the binding constants with the ΔT_m method, FID plots, and computational models generated with Autodock Vina 1.0. This material is available free of charge via the Internet at http://pubs.acs.org.

AUTHOR INFORMATION

Corresponding Author

*Department of Chemistry, Clemson University, Clemson, SC 29634. Telephone: (864) 656-1106. Fax: (864) 656-6613. E-mail: dparya@clemson.edu.

Present Address

†Department of Chemistry, University of the Pacific, Stockton, CA 95211.

Funding

We thank the National Science Foundation (CHE/MCB-0134972) and the National Institutes of Health (R15CA125724) for financial support.

ACKNOWLEDGMENTS

We thank Professor Fenfei Leng (Florida International University, Miami, FL) for providing the software for fitting thermal denaturation profiles using McGhee's model.

ABBREVIATIONS

ITC, isothermal titration calorimetry; DSC, differential scanning calorimetry; FID, fluorescent intercalator displacement; MOPS, 3-(*N*-morpholino)propanesulfonic acid; BPES buffer, 6 mM Na_2HPO_4, 2 mM NaH_2PO_4, and 1 mM Na_2EDTA (pH 7.0); HS, Hoogsteen; WC, Watson−Crick; WH, Watson−Hoogsteen.

REFERENCES

(1) Arya, D. P. (2007) *Aminoglycoside Antibiotics: From Chemical Biology to Drug Discovery*, Wiley-Interscience, Hoboken, NJ.

(2) Fourmy, D., Recht, M. I., Blanchard, S. C., and Puglisi, J. D. (1996) Structure of the A Site of *Escherichia coli* 16S Ribosomal RNA Complexed with an Aminoglycoside Antibiotic. *Science 274*, 1367–1371.

(3) Carter, A. P., Clemons, W. M., Brodersen, D. E., Morgan-Warren, R. J., Wimberly, B. T., and Ramakrishnan, V. (2000) Functional Insights from the Structure of the 30S Ribosomal Subunit and its Interactions with Antibiotics. *Nature 407*, 340–348.

(4) Vicens, Q., and Westhof, E. (2003) Molecular Recognition of Aminoglycoside Antibiotics by Ribosomal RNA and Resistance Enzymes: An Analysis of X-Ray Crystal Structures. *Biopolymers 70*, 42–57.

(5) Kumar, S., Xue, L., and Arya, D. P. (2011) Neomycin-Neomycin Dimer: An all-Carbohydrate Scaffold with High Affinity for AT-Rich DNA Duplexes. *J. Am. Chem. Soc. 133*, 7361–7375.

(6) Xi, H., Kumar, S., Dosen-Micovic, L., and Arya, D. P. (2010) Calorimetric and Spectroscopic Studies of Aminoglycoside Binding to AT-Rich DNA Triple Helices. *Biochimie 92*, 514–529.

(7) Kaul, M., and Pilch, D. S. (2002) Thermodynamics of Aminoglycoside-rRNA Recognition: The Binding of Neomycin-Class Aminoglycosides to the A Site of 16S rRNA. *Biochemistry 41*, 7695–7706.

(8) Fourmy, D., Recht, M. I., and Puglisi, J. D. (1998) Binding of Neomycin-Class Aminoglycoside Antibiotics to the A-Site of 16S rRNA. *J. Mol. Biol. 277*, 347–362.

(9) Willis, B., and Arya, D. P. (2006) An Expanding View of Aminoglycoside-Nucleic Acid Recognition. *Adv. Carbohydr. Chem. Biochem. 60*, 251–302.

(10) Arya, D. P. (2005) Aminoglycoside-Nucleic Acid Interactions: The Case for Neomycin. *Top. Curr. Chem. 253*, 149–178.

(11) Chiang, S., Welch, J., Rauscher, F. J., and Beerman, T. A. (1994) Effects of Minor Groove Binding Drugs on the Interaction of TATA Box Binding Protein and TFIIA with DNA. *Biochemistry (N. Y.) 33*, 7033–7040.

(12) Dorn, A., Affolter, M., Muller, M., Gehring, W. J., and Leupin, W. (1992) Distamycin-induced inhibition of homeodomain–DNA Complexes. *EMBO J. 11 (1)*, 279–286.

(13) Arya, D. P., and Coffee, R. L. Jr. (2000) DNA Triple Helix Stabilization by Aminoglycoside Antibiotics. *Bioorg. Med. Chem. Lett. 10*, 1897–1899.

(14) Le Doan, T., Perrouault, L., Praseuth, D., Habhoub, N., Decout, J. L., Thuong, N. T., Lhomme, J., and Hélène, C. (1987) Sequence-specific recognition, photocrosslinking and cleavage of the DNA double helix by an oligo-[α]-thymidylate covalently linked to an azidoproflavine derivative. *Nucleic Acids Res. 15*, 7749–7760.

(15) Wang, G., Seidman, M. M., and Glazer, P. M. (1996) Mutagenesis in Mammalian Cells Induced by Triple Helix Formation and Transcription-Coupled Repair. *Science 271*, 802–805.

(16) Moser, H. E., and Dervan, P. B. (1987) Sequence-specific cleavage of double helical DNA by triple helix formation. *Science 238*, 645–650.

(17) Perry, P. J., Reszka, A. P., Wood, A. A., Read, M. A., Gowan, S. M., Dosanjh, H. S., Trent, J. O., Jenkins, T. C., Kelland, L. R., and Neidle, S. (1998) Human Telomerase Inhibition by Regioisomeric Disubstituted Amidoanthracene-9,10-Diones. *J. Med. Chem. 41*, 4873–4884.

(18) Sun, D., Thompson, B., Cathers, B. E., Salazar, M., Kerwin, S. M., Trent, J. O., Jenkins, T. C., Neidle, S., and Hurley, L. H. (1997) Inhibition of Human Telomerase by a G-Quadruplex-Interactive Compound. *J. Med. Chem. 40*, 2113–2116.

(19) Izbicka, E., Wheelhouse, R. T., Raymond, E., Davidson, K. K., Lawrence, R. A., Sun, D., Windle, B. E., Hurley, L. H., and Von Hoff, D. D. (1999) Effects of Cationic Porphyrins as G-Quadruplex Interactive Agents in Human Tumor Cells. *Cancer Res. 59*, 639–644.

(20) Barbieri, C. M., Li, T. K., Guo, S., Wang, G., Shallop, A. J., Pan, W., Yang, G., Gaffney, B. L., Jones, R. A., and Pilch, D. S. (2003) Aminoglycoside Complexation with a DNA·RNA Hybrid Duplex: The Thermodynamics of Recognition and Inhibition of RNA Processing Enzymes. *J. Am. Chem. Soc. 125*, 6469–6477.

(21) Arya, D. P., Coffee, R. L. Jr., Willis, B., and Abramovitch, A. I. (2001) Aminoglycosides-Nucleic Acid Interactions: Remarkable Stabilization of DNA and RNA Triple Helices by Neomycin. *J. Am. Chem. Soc. 123*, 5385–5395.

(22) Arya, D. P., Coffee, R. L., and Charles, I. (2001) Neomycin-Induced Hybrid Triplex Formation. *J. Am. Chem. Soc. 123*, 11093–11094.

(23) Xue, L., Xi, H., Kumar, S., Gray, D., Davis, E., Hamilton, P., Skriba, M., and Arya, D. P. (2010) Probing the Recognition Surface of a DNA Triplex: Binding Studies with Intercalator-Neomycin Conjugates. *Biochemistry 49*, 5540–5552.

(24) Ranjan, N., Andreasen, K. F., Kumar, S., Hyde-Volpe, D., and Arya, D. P. (2010) Aminoglycoside Binding to *Oxytricha nova* Telomeric DNA. *Biochemistry 49*, 9891–9903.

(25) Arya, D. P., Micovic, L., Charles, I., Coffee, R. L. Jr., Willis, B., and Xue, L. (2003) Neomycin Binding to Watson-Hoogsteen (W-H) DNA Triplex Groove: A Model. *J. Am. Chem. Soc. 125*, 3733–3744.

(26) Jin, E., Katritch, V., Olson, W. K., Kharatisvili, M., Abagyan, R., and Pilch, D. S. (2000) Aminoglycoside Binding in the Major Groove of Duplex RNA: The Thermodynamic and Electrostatic Forces that Govern Recognition. *J. Mol. Biol. 298*, 95–110.

(27) Arya, D. P., Xue, L., and Willis, B. (2003) Aminoglycoside (Neomycin) Preference is for A-Form Nucleic Acids, Not just RNA: Results from a Competition Dialysis Study. *J. Am. Chem. Soc. 125*, 10148–10149.

(28) Charles, I., Xue, L., and Arya, D. P. (2002) Synthesis of Aminoglycoside-DNA Conjugates. *Bioorg. Med. Chem. Lett. 12*, 1259–1262.

(29) Arya, D. P., Coffee, R. L. Jr., and Xue, L. (2004) From Triplex to B-Form Duplex Stabilization: Reversal of Target Selectivity by Aminoglycoside Dimers. *Bioorg. Med. Chem. Lett. 14*, 4643–4646.

(30) Shaw, N. N., Xi, H., and Arya, D. P. (2008) Molecular Recognition of a DNA:RNA Hybrid: Sub-Nanomolar Binding by a Neomycin-Methidium Conjugate. *Bioorg. Med. Chem. Lett. 18*, 4142–4145.

(31) Zhou, J., Wang, G., Zhang, L. H., and Ye, X. S. (2006) Modifications of Aminoglycoside Antibiotics Targeting RNA. *Med. Res. Rev. 27*, 279–316.

(32) Quader, S., Boyd, S. E., Jenkins, I. D., and Houston, T. A. (2007) Multisite Modification of Neomycin B: Combined Mitsunobu and Click Chemistry Approach. *J. Org. Chem. 72*, 1962–1979.

(33) Arya, D. P., and Willis, B. (2003) Reaching into the Major Groove of B-DNA: Synthesis and Nucleic Acid Binding of a Neomycin-Hoechst 33258 Conjugate. *J. Am. Chem. Soc. 125*, 12398–12399.

(34) Arya, D. P., Xue, L., and Tennant, P. (2003) Combining the Best in Triplex Recognition: Synthesis and Nucleic Acid Binding of a BQQ-Neomycin Conjugate. *J. Am. Chem. Soc. 125*, 8070–8071.

(35) McGhee, J. D. (1976) Theoretical Calculations of the Helix-Coil Transition of DNA in the Presence of Large, Cooperatively Binding Ligands. *Biopolymers 15*, 1345–1375.

(36) Doyle, M. L., Brigham-Burke, M., Blackburn, M. N., Brooks, I. S., Smith, T. M., Newman, R., Reff, M., Stafford, W. F. III, Sweet, R. W., Truneh, A., Hensley, P., and O'Shannessy, D. J. (2000) Measurement of Protein Interaction Bioenergetics: Application to Structural Variants of Anti-sCD4 Antibody. *Methods Enzymol. 323*, 207–230.

(37) Trott, O., and Olson, A. J. (2010) AutoDock Vina: Improving the Speed and Accuracy of Docking with a New Scoring Function, Efficient Optimization, and Multithreading. *J. Comput. Chem. 31*, 455–461.

(38) Pedretti, A., Villa, L., and Vistoli, G. (2004) VEGA: An Open Platform to Develop Chemo-Bio-Informatics Applications, using Plug-in Architecture and Script Programming. *J. Comput.-Aided Mol. Des. 18*, 167–173.

(39) Sanner, M. F. (1999) Python: A Programming Language for Software Integration and Development. *J. Mol. Graphics Modell. 17*, 57−61.
(40) Boger, D. L., Fink, B. E., Brunette, S. R., Tse, W. C., and Hedrick, M. P. (2001) A Simple, High-Resolution Method for Establishing DNA Binding Affinity and Sequence Selectivity. *J. Am. Chem. Soc. 123*, 5878−5891.
(41) Ren, J., and Chaires, J. (1999) Sequence and Structural Selectivity of Nucleic Acid Binding Ligands. *Biochemistry 38*, 16067−16075.
(42) Baruah, H., and Bierbach, U. (2003) Unusual Intercalation of acridin-9-ylthiourea into the 5′-GA/TC DNA Base Step from the Minor Groove: Implications for the Covalent DNA Adduct Profile of a Novel platinum−intercalator Conjugate. *Nucleic Acids Res. 31*, 4138−4146.
(43) Sanger, W. (1983) in *Principles of Nucleic Acid Structure* (Cantor, C. R., Ed.) Springer-Verlag, New York.
(44) Zimmerman, S. B., and Pheiffer, B. H. (1981) A RNA·DNA Hybrid that can Adopt Two Conformations: An X-ray Diffraction Study of Poly(rA)·Poly(dT) in Concentrated Solution or in Fibers. *Proc. Natl. Acad. Sci. U.S.A. 78*, 78−82.
(45) Stefl, R., Trantirek, L., Vorlickova, M., Koca, J., Sklenar, V., and Kypr, J. (2001) A-Like Guanine-Guanine Stacking in the Aqueous DNA Duplex of d(GGGGCCCC). *J. Mol. Biol. 307*, 513−524.
(46) Kypr, J., Fialova, M., Chladkova, J., Tumova, M., and Vorlickova, M. (2001) Conserved Guanine-Guanine Stacking in Tetraplex and Duplex DNA. *Eur. Biophys. J. 30*, 555−558.
(47) Xi, H., Gray, D., Kumar, S., and Arya, D. P. (2009) Molecular Recognition of Single-Stranded RNA: Neomycin Binding to Poly(A). *FEBS Lett. 583*, 2269−2275.
(48) Yadav, R. C., Kumar, G. S., Bhadra, K., Giri, P., Sinha, R., Pal, S., and Maiti, M. (2005) Berberine, a Strong Polyriboadenylic Acid Binding Plant Alkaloid: Spectroscopic, Viscometric, and Thermodynamic Study. *Bioorg. Med. Chem. 13*, 165−174.
(49) Giri, P., Hossain, M., and Kumar, G. S. (2006) Molecular Aspects on the Specific Interaction of Cytotoxic Plant Alkaloid Palmatine to Poly(A). *Int. J. Biol. Macromol. 39*, 210−221.
(50) Xing, F., Song, G., Ren, J., Chaires, J. B., and Qu, X. (2005) Molecular Recognition of Nucleic Acids: Coralyne Binds Strongly to Poly(A). *FEBS Lett. 579*, 5035−5039.
(51) Kankia, B. I. (2003) Mg^{2+}-Induced Triplex Formation of an Equimolar Mixture of Poly(rA) and Poly(rU). *Nucleic Acids Res. 31*, 5101−5107.
(52) Saenger, W. (1984) in *Principle of Nucleic Acid Structure* (Cantor, C. R., Ed.) pp 311, Springer-Verlag, New York.
(53) Rabczenko, A., and Shugar, D. (1971) Studies on the Conformation of Nucleosides, Dinucleoside Monophosphates and Homopolynucleotides Containing Uracil or Thymine Base Residues, and Ribose, Deoxyribose or 2′-O-Methylribose. *Acta Biochim. Pol. 18*, 387−402.
(54) Zimmerman, S. B. (1976) Letter to the Editor: The Polyuridylic Acid Complex with Polyamines: An X-ray Fiber Diffraction Observation. *J. Mol. Biol. 101*, 563−565.
(55) Langridge, R. (1969) Nucleic Acids and Polynucleotides. *J. Cell. Physiol. 74* (Suppl. 1), 1−20.
(56) Bram, S. (1971) Polynucleotide Polymorphism in Solution. *Nat. New Biol. 233*, 161−164.
(57) Nishimura, Y., Torigoe, C., and Tsuboi, M. (1986) Salt Induced B → A Transition of Poly(dG)·Poly(dC) and the Stabilization of A Form by its Methylation. *Nucleic Acids Res. 14*, 2737−2748.
(58) Johnson, D., and Morgan, A. R. (1978) Unique Structures Formed by Pyrimidine-Purine DNAs which may be Four-Stranded. *Proc. Natl. Acad. Sci. U.S.A. 75*, 1637−1641.
(59) Morgan, A. R., and Wells, R. D. (1968) Specificity of the Three-Stranded Complex Formation between Double-Stranded DNA and Single-Stranded RNA Containing Repeating Nucleotide Sequences. *J. Mol. Biol. 37*, 63−80.
(60) Wells, R. D., Larson, J. E., Grant, R. C., Shortle, B. E., and Cantor, C. R. (1970) Physicochemical Studies on Polydeoxyribonucleotides Containing Defined Repeating Nucleotide Sequences. *J. Mol. Biol. 54*, 465−497.
(61) Robinson, H., and Wang, A. H. J. (1996) Neomycin, Spermine and Hexaamminecobalt(III) Share Common Structural Motifs in Converting B- to A-DNA. *Nucleic Acids Res. 24*, 676−682.
(62) Pohl, F. M., and Jovin, T. M. (1972) Salt-Induced Co-Operative Conformational Change of a Synthetic DNA: Equilibrium and Kinetic Studies with Poly(dG-dC). *J. Mol. Biol. 67*, 375−396.
(63) Zhong, W. X., Gulotta, M., Goss, D. J., and Diem, M. (1990) DNA Solution Conformation Via Infrared Circular Dichroism: Experimental and Theoretical Results for B-Family Polymers. *Biochemistry 29*, 7485−7491.
(64) Gulotta, M., Goss, D. J., and Diem, M. (1989) IR Vibrational CD in Model Deoxyoligonucleotides: Observation of the B-Z Phase Transition and Extended Coupled Oscillator Intensity Calculations. *Biopolymers 28*, 2047−2058.
(65) Möller, A., Nordheim, A., Kozlowski, S. A., Patel, D. J., and Rich, A. (1984) Bromination Stabilizes Poly(dG-dC) in the Z-DNA Form Under Low-Salt Conditions. *Biochemistry 23*, 54−62.
(66) Thomas, T. J., Bloomfield, V. A., and Canellakis, Z. N. (1985) Differential Effects on the B-to-Z Transition of Poly(dG-me5dC)·Poly(dG-me5dC) Produced by N1-and N8-Acetyle Spermidine. *Biopolymers 24*, 725−729.
(67) Hasan, R., Alam, M. K., and Ali, R. (1995) Polyamine Induced Z-Conformation of Native Calf Thymus DNA. *FEBS Lett. 368*, 27−30.
(68) Nafisia, S., Sabouryb, A. A., Keramata, N., Neaultc, J. F., and Tajmir-Riahic, H. (2007) Stability and Structural Features of DNA Intercalation with Ethidium Bromide, Acridine Orange and Methylene Blue. *J. Mol. Struct. 827*, 35−43.
(69) Hung, S. H., Yu, Q., Gray, D. M., and Ratliff, R. L. (1994) Evidence from CD Spectra that d(Purine)·r(Pyrimidine) and r(Purine)·d(Pyrimidine) Hybrids are in Different Structural Classes. *Nucleic Acids Res. 22*, 4326−4334.
(70) Ratmeyer, L., Vinayak, R., Zhong, Y. Y., Zon, G., and Wilson, W. D. (1994) Sequence Specific Thermodynamic and Structural Properties for DNA·RNA Duplexes. *Biochemistry 33*, 5298−5304.
(71) Gyi, J. I., Lane, A. N., Conn, G. L., and Brown, T. (1998) Solution Structures of DNA·RNA Hybrids with Purine-Rich and Pyrimidine-Rich Strands: Comparison with the Homologous DNA and RNA Duplexes. *Biochemistry 37*, 73−80.
(72) Kaul, M., Barbieri, C. M., Kerrigan, J. E., and Pilch, D. S. (2003) Coupling of Drug Protonation to the Specific Binding of Aminoglycosides to the A Site of 16 S rRNA: Elucidation of the Number of Drug Amino Groups Involved and Their Identities. *J. Mol. Biol. 326*, 1373−1387.
(73) Gutell, R. R. (1994) Collection of Small Subunit (16S- and 16S-Like) Ribosomal RNA Structures: 1994. *Nucleic Acids Res. 22*, 3502−3507.
(74) Yoshizawa, S., Fourmy, D., and Puglisi, J. D. (1998) Structural Origins of Gentamicin Antibiotic Action. *EMBO J. 17*, 6437−6448.
(75) Vicens, Q., and Westhof, E. (2001) Crystal Structure of Paromomycin Docked into the Eubacterial Ribosomal Decoding A Site. *Structure 9*, 647−658.
(76) Vicens, Q., and Westhof, E. (2002) Crystal Structure of a Complex between the Aminoglycoside Tobramycin and an Oligonucleotide Containing the Ribosomal Decoding A Site. *Chem. Biol. 9*, 747−755.
(77) Ogle, J. M., Brodersen, D. E., Clemons, W. M. Jr., Tarry, M. J., Carter, A. P., and Ramakrishnan, V. (2001) Recognition of Cognate Transfer RNA by the 30s Ribosomal Subunit. *Science 292*, 897−902.
(78) Warner, R. C. (1956) Ultraviolet Spectra of Enzymatically Synthesized Polynucleotides. *Fed. Proc. 15*, 379.
(79) Stevens, C. L., and Felsenfeld, G. (1964) The Conversion of Two-Stranded Poly(A+U) to Three-Stranded Poly(A+2U) and Poly A by Heat. *Biopolymers 2*, 293−314.
(80) Warner, R. C. (1963) in *Informational Macromolecules* (Vogel, H. J., Bryson, V., and Lampen, J. O., Eds.) pp 146, Academic Press, New York.

(81) Fresco, J. R. (1963) in *Informational Macromolecules* (Vogel, H. J., Bryson, V., and Lampen, J. O., Eds.) pp 121−148, Academic Press, New York.
(82) Miles, H. T., and Frazier, J. (1964) Infrared Study of Helix Strandedness in the Poly A-Poly U System. *Biochem. Biophys. Res. Commun. 14*, 21−28.
(83) Blake, R. D., and Fresco, J. R. (1966) Polynucleotides. VII. Spectrophotometric Study of the Kinetics of Formation of the Two-Stranded Helical Complex Resulting from the Interaction of Polyriboadenylate and Polyribouridylate. *J. Mol. Biol. 19*, 145−160.
(84) Bishop, G. R., Ren, J., Polander, B. C., Jeanfreau, B. D., Trent, J. O., and Chaires, J. B. (2007) Energetic Basis of Molecular Recognition in a DNA Aptamer. *Biophys. Chem. 126*, 165−175.
(85) Dadarlat, V. M., and Saxena, V. K. (1998) Stability of Triple-Helical Poly(dT)-Poly(dA)-Poly(dT) DNA with Counterions. *Biophys. J. 75*, 70−91.
(86) Macaya, R., Wang, E., Schultze, P., Sklenar, V., and Feigon, J. (1992) Proton Nuclear Magnetic Resonance Assignments and Structural Characterization of an Intramolecular DNA Triplex. *J. Mol. Biol. 225*, 755−773.
(87) Duca, M., Vekhoff, P., Oussedik, K., Halby, L., and Arimondo, P. B. (2008) The Triple Helix: 50 Years Later, the Outcome. *Nucleic Acids Res. 36*, 5123−5138.
(88) Das, S., Kumar, G. S., Ray, A., and Maiti, M. (2003) Spectroscopic and Thermodynamic Studies on the Binding of Sanguinarine and Berberine to Triple and Double Helical DNA and RNA Structures. *J. Biomol. Struct. Dyn. 20*, 703−714.
(89) Pilch, D. S., Kirolos, M. A., and Breslauer, K. J. (1995) Berenil Binding to Higher Ordered Nucleic Acid Structures: Complexation with a DNA and RNA Triple Helix. *Biochemistry 34*, 16107−16124.
(90) Saenger, W. (1984) in *Principles of Nucleic Acid Structure* (Cantor, C. R., Ed.) pp 311, Springer-Verlag, New York.
(91) Monchaud, D., and Teulade Fichou, M. P. (2008) A Hitchhiker's Guide to G-Quadruplex Ligands. *Org. Biomol. Chem. 6*, 627−36.
(92) Haq, I., Trent, J. O., Chowdhry, B. Z., and Jenkins, T. C. (1999) Intercalative G-Tetraplex Stabilization of Telomeric DNA by a Cationic Porphyrin. *J. Am. Chem. Soc. 121*, 1768−1779.
(93) Freyer, M. W., Buscaglia, R., Kaplan, K., Cashman, D., Hurley, L. H., and Lewis, E. A. (2007) Biophysical Studies of the c-MYC NHE III1 Promoter: Model Quadruplex Interactions with a Cationic Porphyrin. *Biophys. J. 92*, 2007−2015.
(94) Cosconati, S., Marinelli, L., Trotta, R., Virno, A., Mayol, L., Novellino, E., Olson, A. J., and Randazzo, A. (2009) Tandem Application of Virtual Screening and NMR Experiments in the Discovery of Brand New DNA Quadruplex Groove Binders. *J. Am. Chem. Soc. 131*, 16336−16337.
(95) Smith, F. W., and Feigon, J. (1992) Quadruplex Structure of *Oxytricha* Telomeric DNA Oligonucleotides. *Nature 356*, 164−168.
(96) Schultze, P., Hud, N., Smith, F., and Feigon, J. (1999) The Effect of Sodium, Potassium and Ammonium Ions on the Conformation of the Dimeric Quadruplex Formed by the *Oxytricha nova* Telomere Repeat Oligonucleotide $d(G_4T_4G_4)$. *Nucleic Acids Res. 27*, 3018−3028.
(97) Balagurumoorthy, P., Brahmachari, S. K., Mohanty, D., Bansal, M., and Sasisekharan, V. (1992) Hairpin and Parallel Quartet Structures for Telomeric Sequences. *Nucleic Acids Res. 20*, 4061−4067.
(98) Wang, Y., and Patel, D. J. (1993) Solution Structure of the Human Telomeric Repeat $d[AG_3(T_2AG_3)_3]$ G-Tetraplex. *Structure 1*, 263−282.
(99) Leroy, J. L., Gueron, M., Mergny, J. L., and Helene, C. (1994) Intramolecular Folding of a Fragment of the Cytosine-Rich Strand of Telomeric DNA into an i-Motif. *Nucleic Acids Res. 22*, 1600−1606.
(100) Manzini, G., Yathindra, N., and Xodo, L. E. (1994) Evidence for Intramolecularly Folded i-DNA Structures in Biologically Relevant CCC-Repeat Sequences. *Nucleic Acids Res. 22*, 4634−4640.
(101) Spolar, R. S., and Record, M. T. Jr. (1994) Coupling of Local Folding to Site-Specific Binding of Proteins to DNA. *Science 263*, 777−784.
(102) Ha, J. H., Spolar, R. S., and Record, M. T. Jr. (1989) Role of the Hydrophobic Effect in Stability of Site-Specific Protein-DNA Complexes. *J. Mol. Biol. 209*, 801−816.
(103) Haq, I. (2002) Thermodyanmics of Drug-DNA Interactions. *Arch. Biochem. Biophys. 403*, 1−15.
(104) Spolar, R. S., Livingstone, J. R., and Record, M. T. Jr. (1992) Use of Liquid Hydrocarbon and Amide Transfer Data to Estimate Contributions to Thermodynamic Functions of Protein Folding from the Removal of Nonpolar and Polar Surface from Water. *Biochemistry 31*, 3947−3955.
(105) Bergqvist, S., Williams, M. A., O'Brien, R., and Ladbury, J. E. (2004) Heat Capacity Effects of Water Molecules and Ions at a Protein-DNA Interface. *J. Mol. Biol. 336*, 829−842.
(106) Ferrari, M. E., and Lohman, T. M. (1994) Apparent Heat Capacity Change Accompanying a Nonspecific Protein-DNA Interaction. *Escherichia coli* SSB Tetramer Binding to Oligodeoxyadenylates. *Biochemistry 33*, 12896−12910.
(107) Peters, W. B., Edmondson, S. P., and Shriver, J. W. (2004) Thermodynamics of DNA Binding and Distortion by the Hyperthermophile Chromatin Protein Sac7d. *J. Mol. Biol. 343*, 339−360.
(108) Barbieri, C. M., and Pilch, D. S. (2006) Complete Thermodynamic Characterization of the Multiple Protonation Equilibria of the Aminoglycoside Antibiotic Paromomycin: A Calorimetric and Natural Abundance ^{15}N NMR Study. *Biophys. J. 90*, 1338−1349.
(109) Leng, F., Chaires, J. B., and Waring, M. J. (2003) Energetics of Echinomycin Binding to DNA. *Nucleic Acids Res. 31*, 6191−6197.
(110) Ragazzon, P. A., Garbett, N. C., and Chaires, J. B. (2007) Competition Dialysis: A Method for the Study of Structural Selective Nucleic Acid Binding. *Methods 42*, 173−182.
(111) Chaires, J. B. (2005) Competition Dialysis: An Assay to Measure the Structural Selectivity of Drug-Nucleic Acid Interactions. *Curr. Med. Chem.: Anti-Cancer Agents 5*, 339−352.
(112) Chaires, J. B. (2006) A Thermodynamic Signature for Drug-DNA Binding Mode. *Arch. Biochem. Biophys. 453*, 26−31.
(113) Rohs, R., Jin, X., West, S. M., Joshi, R., Honig, B., and Mann, R. S. (2010) Origins of Specificity in Protein-DNA Recognition. *Annu. Rev. Biochem. 79*, 233−269.
(114) Rohs, R., West, S. M., Sosinsky, A., Liu, P., Mann, R. S., and Honig, B. (2009) The Role of DNA Shape in Protein-DNA Recognition. *Nature 461*, 1248−1253.
(115) Parker, S. C., and Tullius, T. D. (2011) DNA Shape, Genetic Codes, and Evolution. *Curr. Opin. Struct. Biol. 21*, 342−347.
(116) Parker, S. C., Hansen, L., Abaan, H. O., Tullius, T. D., and Margulies, E. H. (2009) Local DNA Topography Correlates with Functional Noncoding Regions of the Human Genome. *Science 324*, 389−392.